TSC2 loss in neural progenitor cells suppresses translation of ASD/NDD-associated transcripts in an mTORC1- and MNK1/2-reversible fashion

Pauline Martin,[1, 5] Krzysztof J. Szkop,[2, 5] Francis Robert,[3, 5] Srirupa Bhattacharyya,[1] Roberta L. Beauchamp,[1] Jacob Brenner, [1] Nicholas E. Redmond[1], Sidong Huang,[3] Serkan Erdin,[1 4] Ola Larsson,[2*] Vijaya Ramesh[1*§]

[1]Center for Genomic Medicine, Department of Neurology, Massachusetts General Hospital, Boston, MA 02114, USA; [2]Department of Oncology-Pathology, Science for Life Laboratory, Karolinska Institute, Stockholm 171 77, Sweden; [3]Department of Biochemistry and Goodman Cancer Research Institute, McGill University, Montreal, PQ H3G1Y6, Canada; [4] Program in Medical and Population Genetics, Broad Institute of Harvard and MIT, Cambridge, MA 02142, USA; [5]These authors contributed equally to this work.

* Co-corresponding, equally contributing senior authors: Ola Larsson (ola.larsson@ki.se), Vijaya Ramesh (ramesh@helix.mgh.harvard.edu)

[§] **Lead contact:** Vijaya Ramesh, 185 Cambridge Street, Boston, MA 02114. Phone: 617-724-9733; Email: ramesh@helix.mgh.harvard.edu

SUMMARY

Tuberous sclerosis complex (TSC) is an inherited neurodevelopmental disorder (NDD) with frequent manifestations of epilepsy and autism spectrum disorder (ASD). TSC is caused by inactivating mutations in *TSC1* or *TSC2* tumor suppressor genes, with encoded proteins hamartin (TSC1) and tuberin (TSC2) forming a functional complex inhibiting mechanistic target of rapamycin complex 1 (mTORC1) signaling. This has led to treatment with allosteric mTORC1 inhibitor rapamycin analogs ("rapalogs") for TSC tumors; however, rapalogs are ineffective for treating neurodevelopmental manifestations. mTORC1 signaling controls protein synthesis by regulating formation of the eIF4F complex, with further modulation by MNK1/2 kinases via phosphorylation of the eIF4F subunit eIF4E. While both these pathways modulate translation, comparing their impact on transcriptome-wide mRNA translation, as well as effects of inhibiting these pathways in TSC has not been explored. Here, employing CRISPR-modified, isogenic TSC2 patient-derived neural progenitor cells (NPCs), we have examined transcriptome-wide changes in mRNA translation upon *TSC2* loss. Our results reveal dysregulated translation in *TSC2*-Null NPCs, which significantly overlaps with the translatome from *TSC1*-Null NPCs. Interestingly, numerous non-monogenic ASD-, NDD- and epilepsy-associated genes identified in patients harboring putative loss-of-function mutations, were translationally suppressed in *TSC2*-Null NPCs. Importantly, translation of these ASD- and NDD-associated genes was reversed upon inhibition of either mTORC1 or MNK1/2 signaling using RMC-6272 or eFT-508, respectively. This study establishes the importance of mTORC1-eIF4F- and MNK-eIF4E-sensitive mRNA translation in TSC, ASD and other neurodevelopmental disorders laying the groundwork for evaluating drugs in clinical development that target these pathways as a treatment strategy for these disorders.

INTRODUCTION

Tuberous sclerosis complex (TSC [MIM: 191100 and MIM: 613254]) is an autosomal dominant neurodevelopmental disorder (NDD) with clinical involvement of multiple organ

55 systems including the central nervous system (CNS). TSC is caused by mutations in the *TSC1*
56 [MIM: 605284] or *TSC2* [MIM: 191092] gene, encoding the tumor suppressor protein hamartin
57 (TSC1) or tuberin (TSC2), respectively. In addition to slow growing hamartomas in many
58 organs, neurodevelopmental manifestations such as epilepsy, intellectual disability and autism
59 spectrum disorders (ASD) are commonly observed in these patients [1-3]. TSC proteins function
60 as a complex, relaying signals from diverse cellular pathways to control mechanistic target of
61 rapamycin (mTOR [MIM: 601231]) complex 1 (mTORC1) signaling. Loss of TSC1/TSC2
62 proteins results in aberrant activation of mTORC1, which has led to first-generation mTORC1
63 rapalog inhibitors, emerging as a lifelong therapy for TSC hamartomas [4-7]. Moreover, recent
64 clinical trials reveal that rapalogs reduce epilepsy in 40% of TSC patients [8]. In contrast,
65 rapalogs are ineffective in treating TSC-associated neuropsychiatric disorders (TAND) and
66 autism [9; 10].

67 Among its many activities, mTORC1 signaling plays an essential role in protein synthesis
68 by regulating the efficiency whereby mRNAs are translated into proteins. Aberrant activation
69 of mTORC1, as seen with TSC1/TSC2 loss, leads to hyperphosphorylation of key substrates
70 controlling translation including eukaryotic translation initiation factor (eIF) 4E-binding proteins
71 (4E-BPs [MIM: 602223 and MIM: 602224]) and p70 ribosomal protein S6 kinase 1 (S6K1 [MIM:
72 608938]). In the unphosphorylated state, i.e. when mTORC1 activity is low, 4E-BPs bind and
73 sequester eIF4E [MIM: 133440]. This leads to reduced formation of the heterotrimeric eIF4F-
74 complex, a key factor for initiation of translation, comprised of eIF4E, eIF4G [MIM: 600495]
75 and eIF4A [MIM: 602641]. Activation of mTORC1 leads to phosphorylation of 4E-BPs and
76 thereby release of eIF4E, which promotes eIF4F-complex formation and stimulates 5' cap-
77 dependent translation (Figure 1A). Phosphorylation of S6K protein affects protein synthesis
78 and ribosome biogenesis through multiple mechanisms, including release of sequestered
79 eIF4A via phosphorylation/inactivation of programmed cell death 4 (PDCD4 [MIM: 608610])
80 (Figure 1A) reviewed in [11; 12]. Importantly, mTORC1 modulates translation, and thereby molds
81 the proteome, in a transcript-selective fashion depending on features in the 5' untranslated

82 regions (UTRs) of target mRNAs. Three main classes of transcripts showing translation
83 paralleling mTORC1 activity have been described: mRNAs with very short 5'UTRs, highly
84 structured 5'UTRs and those with the 5′ terminal oligopyrimidine (5′ TOP) motif (reviewed in
85 [13]). Activation of mTORC1 is reported to be associated with suppressed translation of a set of
86 mRNAs commonly harboring upstream open reading frames in their 5'UTRs [14]. In addition,
87 phosphorylation of eIF4E at a single conserved serine (S209) by mitogen-activated protein
88 kinase-interacting kinase MNK1/2 [MIM: 606724 and MIM: 605069] also modulates translation
89 in a transcript-selective fashion (Figure 1A) [15; 16].

90 Although commonly used rapalogs efficiently suppress phosphorylation of S6K1, they only
91 marginally affect 4E-BP1 phosphorylation in many cell types, which is consistent with rapalogs
92 only partially inhibiting mTORC1 activity [17-19]. This prompted the development of third-
93 generation bi-steric mTORC1-selective inhibitors, Rapalinks, that link the mTORC1 affinity of
94 rapamycin with a potent second-generation active-site mTOR kinase inhibitor, resulting in
95 reduced phosphorylation of both S6K1 and 4E-BP1 [20]. A more recent third-generation bi-steric
96 mTORC1-selective inhibitor, RMC-6272 (a preclinical tool compound for its clinical counterpart
97 RMC-5552), shows dramatically improved mTORC1 selectivity as compared to the Rapalink
98 prototype while potently reducing phosphorylation of both S6K1 and 4E-BP1 (Figure 1A) [21; 22].
99 Moreover, we recently demonstrated that RMC-6272 is superior to rapamycin in durably
100 inhibiting the mTORC1-4E-BP1 axis and suppressing tumor growth in patient-derived *NF2*-
101 deficient models [23]. RMC-6272 has also shown strong anti-tumor activity as a single agent or
102 when combined with other treatments in several preclinical cancer models [21], and the first-in-
103 human study of RMC-5552 has offered preliminary data of anti-tumor activity at tolerated
104 doses (NCT04774952 and Schram et al., 2023 https://doi.org/10.1158/1535-7163.TARG-23-
105 C020). Additionally, recently developed eFT-508/tomivosertib is a potent and selective
106 MNK1/2 inhibitor that effectively blocks phosphorylation of eIF4E (Figure 1A) [24] and is in phase
107 2 clinical trials for several cancer types (NCT02937675, NCT02605083 and NCT03258398).

108 While numerous global studies of mRNA levels ("transcriptomes") in patient-derived
109 neuronal models of ASD, TSC and other NDDs have been reported, studies of mRNA
110 translation are largely lacking. Furthermore, the effects on mRNA translation from highly
111 specific mTORC1 and MNK inhibitors such as RMC-6272 and eFT-508 in NDDs have never
112 been explored. Our recent studies employing polysome-profiling to examine mRNA translation
113 at a transcriptome-wide level in TSC1 patient-derived neural progenitor cells (NPCs)
114 uncovered *TSC1*-associated transcript-selective alterations in translation that were largely
115 insensitive to rapamycin. Interestingly, in confirmational studies using NanoString analysis, we
116 observed that a small subset of selected mRNAs encoding proteins related to synaptic
117 regulation or ASD were rapamycin-insensitive but showed sensitivity to RMC-6272. Moreover,
118 unlike rapamycin, RMC-6272 also reversed some of the neurodevelopmental phenotypic
119 defects in *TSC1*-Null NPCs [25]. These findings suggest a key role of mTORC1-4E-BP1-eIF4E
120 axis-dependent modulation of mRNA translation in TSC. Here, we have further investigated
121 the role of this axis in regulating mRNA translation using an isogenic set of CRISPR-modified
122 TSC2 patient-derived NPCs. Our results reveal a strong overlap in dysregulated translation
123 observed in *TSC1*-Null and *TSC2*-Null NPCs. Surprisingly, genes previously associated with
124 ASD and NDD were translationally suppressed in *TSC2*-Null NPCs, and their translation was
125 reversed upon RMC-6272 or eFT-508 treatment. These results establish the importance of
126 mTORC1-eIF4F- and MNK-eIF4E-mediated mRNA translation in TSC, ASD and NDDs and
127 lay the groundwork for evaluating drugs in clinical development that target these pathways as
128 a treatment strategy for TAND as well as ASD/NDD.
129

130 **MATERIAL AND METHODS**

131 ***Human induced pluripotent stem cell derivation***

132 We previously reported collection of post-mortem subungal fibroma (SUF) tissue from a
133 female sporadic TSC2 patient, which was obtained through the pathology department and
134 approved by the Institutional Review Board at Massachusetts General Hospital. Detailed

135 genetic analysis of the patient SUF tissue, including exon-by-exon scanning of the entire
136 coding sequence of *TSC2* isoform 1 (GenBank: NM_000548), identified a single heterozygous
137 (*TSC2*-Het) truncating nonsense mutation in *TSC2* exon 34 (originally reported as coding exon
138 33; 4207delG, D1400fs>1410X). Further analysis of the SUF tissue for tumor clonality and
139 loss-of-heterozygosity (LOH), using multiple polymorphic chromosome 16 or *TSC2* intragenic
140 markers, revealed a clonal tumor with no second-hit mutations or LOH [26]. For culturing of
141 primary *TSC2*-Het fibroblasts, at the time of collection SUF tissue was rinsed twice in Hank's
142 Balanced Salt Solution (Sigma) followed by mincing in high glucose DMEM (Gibco) containing
143 15% fetal bovine serum (FBS; Sigma), 0.5 µg/ml fungizone (Life Technologies), 50 g/ml
144 gentamicin (Life Technologies), and 1x penicillin-streptomycin/L-glutamine (Cellgro). The
145 tissue was then digested in the same medium as above (without gentamycin) containing ~5
146 units collagenase III (Fisher Scientific), for 30 min at 37^0C. Digested tissue was then pelleted
147 by centrifugation, resuspended in high glucose DMEM (containing 15%FBS, 1x penicillin-
148 streptomycin/L-glutamine), and the resulting cultured fibroblast line was then expanded and
149 cryopreserved in liquid nitrogen. Following revival of cryopreserved cells, *TSC2*-Het fibroblasts
150 were reprogrammed using synthetic modified mRNA-based methods to obtain induced
151 pluripotent stem cells (iPSCs) as described [27; 28]. Briefly, cells were transfected by nucleo-
152 electroporation (Amaxa Nucleofector I) with *in vitro* transcribed mRNAs encoding *Oct4, Sox2,*
153 *Klf4, c-Myc* and *Lin28* (Stemgent). After single clone picking, iPSC colonies were cultured in
154 feeder-free conditions in Essential 8 medium (ThermoFisher) on plates coated with Geltrex
155 (Gibco) using the "thin gel method" according to the manufacturer's instructions. Colonies
156 were passaged every 4-6 days with daily medium change. Sanger sequencing confirmed the
157 original heterozygous mutation in *TSC2*-Het iPSCs (see details below for *TSC2* exon 34 PCR
158 and sequencing).
159
160 ***CRISPR/Cas9-mediated generation of isogenic iPSC lines***

161 To generate both the corrected-wildtype (WT) and Null isogenic iPSC lines, CRISPR/Cas9
162 genome editing was performed employing parental *TSC2*-Het iPSCs. To achieve gene knock-
163 in to correct the germline *TSC2* mutation, we followed the same cloning and transfection
164 strategy as we previously reported for *TSC1* corrected-WT iPSCs [29]. Briefly, using web-based
165 CRISPR-related tools developed by GenScript (https://www.genscript.com), we designed a
166 single guide RNA (sgRNA): 5'-GGACATCCTCGGGGACCCTG-3' targeting *TSC2* exon 34
167 (coding exon 33) along with an asymmetric donor sequence: 5'-
168 CCGAGGCCGACCAGGCAGCACTTTCCCCGTCCAGGGTCCCTGACTGTGACCGGGCCT
169 TAACCTCAGGGCTCAGCCGGCCCACGTCGGCCTTGTCCCCAGGGTCCCCGAGGATGT
170 CCTGCAGAGTCTGCAG-3' for homology-directed repair. Colonies were manually isolated,
171 and genomic DNA was extracted from a portion of each colony followed by PCR amplification
172 using primers TSC2-ex33F: 5'-CTGACAGGGGTTCTCTTTGG-3' and TSC2-ex33R: 5'-
173 TCCAGGGTCCCTGACTGTGA-3'. Screening by Sanger sequencing, using a nested primer
174 TSC2-ex33-seqF: 5'-TCGTCCTCAGTCTCCAGCC-3', identified one clone with successful
175 correction back to WT. For generating the *TSC2*-Null iPSC lines, we used a service provided
176 by an independent company (Alstem Cell Advancements, Richmond, CA). Briefly, *TSC2*-Het
177 iPSCs were co-transfected by nucleo-electroporation (Amaxa Nucleofector I) with a pair of
178 sgRNAs targeting *TSC2* exon 2 (coding exon 1) including sgRNA-1: 5'-
179 TGTTGGGACTGGGAACACCG-3' and sgRNA-2: 5'-ACTCACTCTCAGTATTTCCG-3'. A total
180 of 50 single clones were screened by PCR amplification and Sanger sequencing using primers
181 TSC2-F2: 5'- CCATGGCCAAACCAACAAG-3' and TSC2-R2: 5'-
182 ACCTGGTGCAAGACCAAA-3', with 3 homozygous *TSC2*-Null clones identified, all of which
183 harbored the same 59 bp deletion in *TSC2* exon 2 resulting in a frameshift and premature
184 protein truncation.
185
186 ***Differentiation of iPSCs into NPCs***

187 To generate NPCs, *TSC2*-iPSCs including the parental *TSC2*-Het line, the single *TSC2*-
188 WT clone and two of the three *TSC2*-Null clones (clones 5 and 39) were differentiated using
189 the directed monolayer differentiation protocol as we previously reported for TSC1-NPCs [29;
190 30]. Briefly, iPSCs expressing the pluripotency marker TRA-1-60 were sorted and enriched
191 using magnetic-activated cell separation (MACS) technology (Miltenyi Biotec). Cells were
192 cultured in neural induction medium (neurobasal medium supplemented with 1x neural
193 induction supplement (ThermoFisher)) for 7-9 days, followed by a second sorting for cells
194 expressing polysialylated-neural cell adhesion molecule (PSA-NCAM). The PSC-NCAM-
195 positive (+) cells then underwent a double-sorting to enrich for NPCs representing CD271(-)
196 /CD133(+) cells. NPCs were then cultured in neural expansion medium (1:1 neurobasal
197 medium:advanced DMEM/F12, 1x neural induction supplements (ThermoFisher) and 1x
198 penicillin/streptomycin (Corning)). MACS sorting was performed using microbead kits for TRA-
199 1-60, PSA-NCAM, CD271 and CD133 (Miltenyi Biotec).
200
201 ***Immunocytochemistry***
202 To confirm successful derivation of NPCs, immunofluorescent staining was carried out
203 using NPC markers Nestin (EMD Millipore) and Sox2 (R&D Systems) antibodies as previously
204 described [29; 30]. Briefly, cells were fixed with 4% paraformaldehyde (PFA; Electron Microscopy
205 Sciences) and then permeabilized and blocked in a single step using PBS containing 4%
206 normal goat serum (NGS)/0.1% Triton-X-100. Primary antibodies were diluted into PBS
207 containing 2% NGS/0.1% Triton-X-100. DAPI (Invitrogen) was used to stain nuclei at 5 μg/ml.
208 Coverslips were mounted in ProLong Gold antifade Mountant (Invitrogen) and images were
209 captured using a Nikon Eclipse TE2000-U microscope and the NIS-Element BR 3.2 imaging
210 software.
211
212 ***Immunoblot analysis***

213 Cells were lysed in RIPA lysis buffer (50 mM Tris (pH7.5), 150 mM NaCl, 0.1% SDS, 0.5%
214 sodium deoxycholate, 1% NP-40, 1x HALT phosphatase inhibitor cocktail (Pierce) and 1x
215 protease inhibitor cocktail (Sigma)) as previously described [31; 32]. Protein lysates were resolved
216 on 4-12% or 10-20% Novex WedgeWell Tris-glycine gels (Invitrogen), transferred to 0.45 μm
217 pore nitrocellulose (BioRad) and then incubated with primary antibodies to detect TSC2, pS6K
218 T389, S6K, pS6 S240/244, S6, p4E-BP1 S65, 4E-BP1, peIF4E S209, and eIF4E (Cell
219 Signaling Technologies); β-actin (Santa Cruz Biotechnology) or GAPDH (EMD Millipore). All
220 immunoblotting data shown are representative of at least 3 biological replicates.
221
222 ***Cell Size and proliferation***
223 Cell size and proliferation were determined for *TSC2*-WT, Het and Null NPCs treated for
224 72 h with 50 nM rapamycin (MilliporeSigma), 10 nM RMC-6272 (generously provided by
225 Revolution Medicines Inc.) or DMSO as vehicle control. For both cell size and proliferation,
226 NPCs were analyzed by trypan blue exclusion using the Countess II automated cell counter
227 (ThermoFisher) as previously described [25; 29]. Briefly, cells were detached using Accutase
228 enzyme detachment medium (ThermoFisher), and for each sample, 10 μl of suspended cells
229 were combined with 10 μl of trypan blue, and then 10 μl of the resulting mixture was assessed
230 using the Countess II automated cell counter (ThermoFisher), according to the manufacturer's
231 instructions. Quantification of viable and dead cells was performed along with size of viable
232 cells. For proliferation, counting of viable cells collected at days (D) 1, 2, 3 and 4 after seeding
233 was performed for cells treated with 50 nM rapamycin, 10 nM RMC-6272 or DMSO on D1. All
234 data collected using the Countess II cell counter were analyzed from 3 independent
235 experiments (3 technical replicates each). Proliferation was further assessed using flow
236 cytometry employing the proliferation marker Ki-67 as previously described [25]. Briefly, *TSC2*-
237 WT, Het and Null NPCs were seeded onto Geltrex-coated plates followed by treatment with
238 50 nM rapamycin, 10 nM RMC-6272, 50 nM eFT-508 (Selleckchem) or DMSO as vehicle

239 control for 72 h (two biological replicates). To assess Ki-67 proliferation status, NPCs were
240 fixed with 4% PFA, permeabilized with ice cold 100% methanol to a final concentration of 90%
241 with gentle vortexing and stained using AlexaFluor (AF) 488-conjugated Ki-67 monoclonal
242 antibody or AF488-conjugated IgG as an isotype control (Cell Signaling Technologies). Data
243 were acquired from ~$1x10^4$ cells using a BD LSR II Flow Cytometer (BD Biosciences), and
244 analysis was carried out using FlowJo 10.8.1 (FlowJo LLC). Percentages of Ki-67 positive
245 cells (acquired through FITC channel) were determined by gating with respect to AF488-IgG
246 control.
247
248 ***Neurite outgrowth assay***
249 NPCs were assessed for neurite outgrowth as previously described [29]. Briefly, NPCs were
250 seeded on coverslips coated with poly-D-lysine (0.1 mg/ml, Sigma) and fibronectin (5 μg/ml,
251 Corning) in growth factor-depleted neural expansion medium containing 1:1 neurobasal
252 medium:advanced DMEM/F12 (ThermoFisher), 0.3x neural induction supplements
253 (ThermoFisher) and 1x penicillin/streptomycin (Corning). Cells were treated with 50 nM
254 rapamycin, 10 nM RMC-6272 or DMSO vehicle control for 48 h followed by fixation with 4%
255 PFA prior to immunostaining. Three independent experiments were performed where images
256 were acquired from 8 non-overlapping fields and analyzed using HCA-Vision software V.2.2.0
257 (CSIRO, Canberra, Australia) [33]. Images were acquired using a Nikon Eclipse TE2000-U
258 microscope and NIS-Element BR 3.2 imaging software.
259
260 ***Polysome fractionation and RNA sequencing***
261 Lysate were prepared for polysome profiling from three biological replicates as previously
262 described with minor modifications [34]. Briefly, TSC2-NPC lines were seeded at ~50,000
263 cells/cm^2, with a total of ~$2.4x10^7$ cells seeded per replicate for three drug treatment
264 conditions, including 10 nM RMC-6272, 50 nM eFT-508 or DMSO control. The day after
265 seeding, cells were treated for 2 h, rinsed with 1x PBS containing 100 μg/ml cycloheximide

266 (CHX) (Sigma), harvested by scraping on ice in PBS/CHX and pelleted by centrifugation at
267 300g for 10 min at + 4C. Cell pellets were first resuspended in hypotonic lysis buffer containing
268 5 mM Tris-HCl (pH 7.5), 2.5 mM $MgCl_2$ and 1.5 mM KCl, followed by addition of DTT (2 mM
269 final), CHX (100 µg/ml final), sodium deoxycholate (0.5% final) and Triton X-100 (0.5% final).
270 Lysates were then vortexed for 4 sec, cleared by spinning for 2 min at 13,000 rpm and quickly
271 frozen on dry ice. When ready for processing, lysates were quickly thawed at 37°C and loaded
272 onto a 10 - 50% sucrose gradient, followed by centrifugation for 2 h and 15 min at 35,000 rpm
273 in a SW41 rotor using a Sorvall Discovery 90SE centrifuge. The gradients were fractionated
274 on a Teledyne ISCO Foxy R1 apparatus while monitoring the OD254nm. Fractions
275 corresponding to mRNA associated with more than two ribosomes were pooled and the RNA
276 extracted using TRIzol (ThermoFisher) according to the manufacturer's protocol. 10% of the
277 lysate was removed from the extract prior to loading on the sucrose gradient, extracted using
278 TRIzol, and denoted as total RNA. RNA sequencing libraries were prepared from the resulting
279 samples (both polysome-associated and total RNA) using Illumina v2.5 Kits and sequenced
280 on an Illumina NextSeq 500 at the Canada's Michael Smith Genome Sciences Centre (BC
281 Cancer Research Institute, Vancouver, Canada).
282
283 ***RNA sequencing data preprocessing and quality control***
284 Adapters were removed from RNA sequencing reads using bbduk.sh from the BBTools
285 software suite [https://www.osti.gov/servlets/purl/1241166] (v. 36.59 with settings: k = 13, ktrim
286 = n, useshortkmers = t, mink = 5, qtrim = t, trimq = 10, minlength = 20). Paired-end reads were
287 aligned to hg38 using HISAT2 [35] (ver 2.1.0 with settings: --no-mixed, --no-discordant), and
288 uniquely mapped reads were quantified using the featureCounts function from the RSubreads
289 package (v.2.6.4) [36] with RefSeq gene definitions and default settings. Polysome-profiling data
290 from the previous study of *TSC1*-dependent translation[25] were quantified using the same gene
291 definitions to allow a direct comparison to the herein generated dataset. Dataset reproducibility

292 was assessed using Principal Component Analysis using genes within the highest quartile of
293 standard deviations quantified across all samples as input.
294
295 ***Analysis of gene expression alterations using anota2seq***
296 Gene expression quantified from polysome-associated and total mRNA was analyzed
297 using the anota2seq algorithm (v. 1.20.0) [37]. Batch effects were accounted for in the models
298 by including sample replicates using the "batchVec" argument in anota2seq. Default threshold
299 settings were used [settings minSlopeTranslation = -1, maxSlopeTranslation = 2,
300 minSlopeBuffering = -2, maxSlopeBuffering = 1, deltaPT = deltaP = deltaTP = deltaT =
301 log2(1.2), minEff=log2(1.5)] with a significance threshold maxRvmPAdj = 0.15 (corresponding
302 to a false discovery rate [FDR] < 0.15). Transcripts were classified into three modes of
303 regulation assessed by anota2seq (changes in mRNA abundance, changes in translation, and
304 translational offsetting) using the "anota2seqRegModes' function.
305
306 ***Analysis of gene signatures using empirical cumulative distribution functions***
307 Empirical cumulative distribution functions (ECDFs) of log2 fold changes for polysome-
308 associated and total mRNA were plotted for gene signatures including ASD and NDD genes
309 [38], eIF4E overexpression [39], mTOR-sensitive genes [40] obtained from previous publications or,
310 to cross-compare datasets, genes that were found to be translationally regulated in either
311 dataset. The Wilcoxon rank-sum test was used to determine whether there was a significant
312 shift between each signature and the background (i.e. genes not within the signature).
313
314 ***Gene set enrichment analysis***
315 Gene Ontology (GO) enrichment analysis was performed using genes classified as
316 regulated via translation by anota2seq (differentially translated genes, "DTGs") and annotation
317 from GO biological process (GO:BP) terms retrieved from MSigDB database (v. 2023.2.Hs) [41]
318 using one-tailed Fisher's exact test. In this analysis, only GO:BP terms with at least 10 genes

319 within the background set (all detected genes analyzed by anoat2seq) of a particular
320 comparison were considered. DTG datasets for GO analysis included *TSC2*-Null vs WT NPCs,
321 *TSC2*-Null NPCs treated with RMC-6272 vs DMSO control, *TSC2*-Null NPCs treated with eFT-
322 508 vs DMSO control, pairwise comparison between *TSC2*-Null NPCs treated with RMC-6272
323 or eFT-508 as well as pairwise comparisons between *TSC2*-Null vs WT NPCs and our
324 previously published dataset comparing *TSC1*-Null vs WT NPCs [25]. In addition, genes were
325 ranked based on fold-changes for translation determined by anota2seq analysis for a given
326 comparison. The analysis utilized ASD-, NDD- and EPI-associated gene sets. This was
327 conducted using the fgsea package (v.1.24.0, https://doi.org/10.18129/B9.bioc.fgsea) within
328 the R environment. For each gene set, the Normalized enrichment score (NES) and FDR were
329 calculated.

330 Enrichment analysis for selected DTGs identified by anota2seq and target gene sets,
331 including ASD-, NDD-, EPI-associated genes [38; 41; 42] and eIF4E-sensitive genes [39], was
332 performed using one-tailed Fisher's exact test. Statistical significance of overlaps between the
333 two DTG datasets was also assessed using one-tailed Fisher's exact test. Here, all anota2seq
334 analyzed genes in a single comparison, or intersection of anota2seq analyzed genes in paired
335 comparisons, constituted the background sets. These enrichment analyses were performed
336 in the R statistical software environment (version 3.4.3) (https://www.R-project.org/) using
337 custom scripts.

338

339 ***Validation of differential translation using RT-qPCR***

340 For validation, polysome fractionations were collected from *TSC2*-Null or *TSC2*-WT NPCs
341 (three biological replicates), and RNA was isolated as described for NPCs above. cDNA was
342 prepared using M-MuLV Reverse Transcriptase (New England Biolabs) and oligo(dT)20
343 primers using the manufacturer's recommendations. RT-qPCRs were performed with SsoFast
344 EvaGreen Supermix using the CFX96 PCR system (Bio-Rad). Primers for RT-qPCR are
345 detailed in Table S1. The level of each mRNA was normalized to β-actin (*ACTB* [MIM: 102630])

346 and Phosphoglycerate Kinase 1 (*PGK1* [MIM: 311800]) using the comparative CT method and
347 compared across conditions as indicated in the figure legend.
348
349 ***Statistical analyses***
350 Methods for statistics are described above, or in corresponding figure legends.
351
352 **RESULTS**
353 ***Establishment of an isogenic set of TSC2 patient-derived neural progenitor* cells**
354 We generated an isogenic set of TSC2 patient-derived NPCs using a similar approach as
355 we described previously for TSC1 patient-derived NPCs [25; 29]. Primary fibroblasts cultured from
356 post-mortem SUF tissue were found to harbor a germline heterozygous 1 bp deletion in *TSC2*
357 exon 34 (originally reported as coding exon 33) with no loss-of-heterozygosity [26]. Induced
358 pluripotent stem cells (iPSCs) were generated from the fibroblasts, followed by CRISPR-
359 based genome editing that demonstrated (i) correction of the heterozygous mutation back to
360 wildtype, or (ii) knock out of the second allele due to a 59 bp deletion in *TSC2* exon 2 (coding
361 exon 1). This resulted in an isogenic set of iPSCs representing the parental *TSC2*-Het line, a
362 single clone of *TSC2*-corrected (*TSC2*-WT) and three clones of *TSC2*-Null iPSCs. We then
363 selected *TSC2*-WT, Het and two Null iPSC clones (clones 5 and 39) for microbead sorting of
364 neural cell surface protein markers to obtain NPCs as previously described [29]. Immunostaining
365 for neural markers Nestin and Sox2 confirmed successful NPC derivation (Figure S1A). Loss
366 of TSC2 protein expression was confirmed in *TSC2*-Null clones when compared with the
367 *TSC2*-WT (Figure S1B). We also observed increased phosphorylation of mTORC1 targets
368 p70S6K (pS6K T389), pS6 S240/244 and p4E-BP1 S65 in both *TSC2*-Null NPC clones
369 compared with *TSC2*-WT NPCs, consistent with activation of mTORC1 signaling, while *TSC2*-
370 Het NPCs revealed only minimal activation of mTORC1, which is in agreement with several
371 reports that employed human iPSC models of TSC [43-46] (Figure S1B). *TSC2*-Null NPCs
372 demonstrated an enlarged cell phenotype compared with *TSC2*-WT cells (Figure 1B, D), which

373 is a hallmark of mTORC1 activation. *TSC2*-Het NPCS exhibited an intermediate cell size
374 phenotype (Figure 1B, D). Treatment with rapamycin or RMC-6272 attenuated
375 phosphorylation of S6K at T389, along with its downstream substrate ribosomal protein S6
376 (pS6 S240/244) and rescued the enlarged cell size (Figure 1C, D). As expected, rapamycin
377 showed only minimal effects on phosphorylation of 4E-BP1 while RMC-6272 demonstrated
378 complete inhibition (Figure 1C). These results are consistent with our observations in TSC1-
379 NPCs [25] and with previous studies showing that the mTORC1-S6K signaling axis controls cell
380 size [47].
381
382 ***Rescue of early neurodevelopmental phenotypes by RMC-6272, but not rapamycin***
383 We previously demonstrated that defects in early neurodevelopmental phenotypes in
384 *TSC1*-Null NPCs, including increases in proliferation rate and neurite outgrowth, could be
385 rescued by RMC-6272 treatment, but not rapamycin. This suggests dependence, at least in
386 part, on the mTORC1-4E-BP1 signaling axis [25; 29]. Here, we assessed proliferation by viable
387 cell count in TSC2-NPCs over the course of four days (D1-4) after seeding, also comprising a
388 72 h treatment with 50 nM rapamycin, 10 nM RMC-6272 or DMSO control initiated at D1. We
389 observed genotype-dependent changes in cell numbers in vehicle-treated cells whereby
390 *TSC2*-Null NPCs showed significantly increased proliferation relative to *TSC2*-WT NPCs with
391 *TSC2*-Het also showing augmented proliferation as compared to *TSC2*-WT NPCs (Figure 2A,
392 left graph region). When compared with DMSO treatment, rapamycin showed no significant
393 effect in *TSC2*-WT, -Het or -Null NPCs (Figure 2A, center compared with left graph regions);
394 whereas RMC-6272 demonstrated significant reduction by D3 in all three NPC genotypes,
395 with the maximal decrease observed in *TSC2*-Null NPCs (Figure 2A, right compared with left
396 graph regions). Consistent with this, flow cytometry-based analysis showed a reduction in the
397 percentage of S phase-positive cells (as indicated by Ki-67 positive staining) in RMC-6272 vs
398 DMSO treated *TSC2*-WT (50.9% vs 62.7%), *TSC2*-Het (56.2% vs 64.9%) and *TSC2*-Null
399 (53.7% vs 68.9%) NPCs. In contrast, similar percentages of Ki-67 positivity were found for

400 rapamycin or DMSO treatment (Figure S2A). Moreover, treatment with eFT-508/tomivosertib,
401 a MNK1/2 inhibitor, which attenuates phosphorylation of eIF4E at S209 (peIF4E S209) but not
402 4E-BP1 (p4E-BP1 S65) did not alter Ki-67 positivity in *TSC2*-Null NPCs (Figure S2A, B).
403 We next assessed neurite outgrowth in isogenic TSC2-NPCs using MAP2 immunostaining
404 and HCA-Vision image analysis software to quantitate three parameters (as an average per
405 cell): (i) length of neurite outgrowth, (ii) number of neurite roots and (iii) number of extremities
406 (terminal endpoint of primary and branched outgrowths). In TSC2-NPCs treated for 48 h with
407 DMSO, a significant increase in neurite length/cell of ~3.2-fold in *TSC2*-Null and an
408 intermediate increase of ~1.4-fold in *TSC2*-Het was observed relative to *TSC2*-WT NPCs
409 (Figure 2B, C). *TSC2*-Null NPCs also revealed a significant increase in neurite number/cell
410 (~1.5-fold) and extremities/cell (~1.7-fold) relative to *TSC2*-WT NPCs (Figure 2B, C). Upon
411 RMC-6272 treatment, we observed decreases in neurite length, number and extremities of
412 0.73, 0.90 and 0.83, respectively, for *TSC2*-Het NPCs, and 0.46, 0.68 and 0.64, respectively,
413 for *TSC2*-Null NPCs (Figure 2D). Similar to the proliferation assays, rapamycin failed to rescue
414 neurite-related phenotypes, and in fact showed an opposite trend in several parameters
415 (Figure 2D). Taken together, these data support that the third-generation mTORC1 inhibitor
416 RMC-6272 more effectively reverses the early neurodevelopmental phenotypes observed in
417 TSC2-NPCs, and that this effect is dependent on a more potent inhibition of mTORC1-4E-BP
418 signaling.
419
420 ***Abundant mRNA translation alterations in* TSC2*-Null NPCs largely overlap with those***
421 ***observed in* TSC1*-Null NPCs***
422 Our findings above demonstrate activation of mTORC1 signaling and increases in
423 proliferation and neurite outgrowth in *TSC2*-Null NPCs, compared with WT cells. As mRNA
424 translation is a major downstream target of mTORC1, it is necessary to study how both mRNA
425 levels and translation are affected by *TSC2* loss to disentangle gene expression-dependent
426 effects on cellular phenotypes. We therefore applied polysome-profiling in *TSC2*-Null and

427 *TSC2*-WT NPCs. Cytoplasmic mRNA was fractionated based on ribosome-association and
428 the resulting polysome-associated (herein mRNA associated with >2 ribosomes) and total
429 cytoplasmic mRNA pools were then quantified using RNA sequencing followed by anota2seq
430 analysis [37; 48]. This allowed identification of *TSC2*-associated alterations in (i) "translation",
431 defined as polysome-associated mRNA alterations not paralleled by corresponding changes
432 in total mRNA levels; (ii) "abundance", representing congruent modulation of total and
433 polysome-associated mRNA; and (iii) "offsetting", defined as alterations in total mRNA not
434 paralleled by corresponding changes in polysome-associated mRNA. This analysis revealed
435 numerous *TSC2*-associated alterations in mRNA translation visualized using a scatterplot
436 comparing *TSC2*-dependent changes in polysome-associated and total mRNA (Figure 3A;
437 Table S4) and densities of p-values and false discovery rates (FDRs) obtained from anota2seq
438 analysis (Figure 3B). These alterations in translation occurred alongside less abundant
439 changes in mRNA levels and essentially in absence of translational offsetting (Figure 3A).
440 Although the analysis is expected to be hampered by the large number of regulated genes,
441 we used gene ontology analysis to identify cellular functions targeted by these changes in
442 translation. This revealed that translationally suppressed transcripts encode proteins enriched
443 for annotation to cellular functions including protein DNA complex organization, chromatin
444 remodeling, RNA metabolism, and cell cycle while those involved in a variety of metabolic
445 processes were translationally activated (Figure 3C).

446 To assess how these *TSC2*-associated alterations in mRNA translation compare to our
447 previously described *TSC1*-associated changes, we looked for differences in the response to
448 loss of *TSC1* vs *TSC2* relative to their respective control conditions (i.e. the interaction effect)
449 using an anota2seq-like approaches we described previously [49]. Strikingly, only one gene
450 showed a statistically significant difference in translation response upon *TSC1* vs *TSC2* loss
451 (at FDR < 0.15), and this analysis therefore argues for largely overlapping effects on mRNA
452 translation. To further assess this, we generated gene signatures of transcripts that were
453 translationally up or downregulated in *TSC1*-Null or *TSC2*-Null NPCs relative to their controls

454 and visualized how these gene sets were regulated across the two models. This revealed that
455 transcripts whose translation was activated or suppressed in *TSC2*-Null NPCs showed similar
456 regulation in *TSC1*-Null NPCs and, vice versa, transcripts whose translation was activated or
457 suppressed in *TSC1*-Null NPCs showed similar regulation in *TSC2*-Null NPCs (Figure 3D).
458 Yet, there were differences in mRNA level changes for these subsets (compare Figure 3D left
459 and right plots) that, together with expected threshold-effects, resulted in a smaller set of 949
460 translationally suppressed and 189 translationally activated transcripts that passed threshold
461 applied in anota2seq for both comparisons (Figure 3E). As expected, these shared genes
462 were enriched in similar gene ontology categories as those identified upon *TSC2* loss (Figure
463 3F). In aggregate, these results indicate extensive remodeling of mRNA translation in *TSC2*-
464 Null NPCs largely recapitulating that observed in *TSC1*-Null NPCs.
465
466 ***Suppressed translation of mRNAs encoding proteins associated with ASD and NDD***
467 ***upon* TSC2 *loss***
468 To explore the relationship between altered gene expression associated with *TSC2* loss
469 and patient phenotypes we reasoned that *TSC2* loss may affect translation of mRNAs
470 encoding proteins implicated in non-syndromic autism spectrum disorder (ASD), general
471 neurodevelopmental disorders (NDD) and/or epilepsy. To assess this, we utilized data from
472 recent studies that identified high confidence *de novo* mutations in large cohorts of individuals
473 diagnosed with ASD, NDD as well as epilepsy. For ASD/NDD-related genes, we used datasets
474 reported by Fu and colleagues, including 72 genes associated with ASD (ASD72) and 373
475 genes associated with NDD (NDD373) identified at a stringent FDR $\leq$ 0.001 threshold, as well
476 as 185 ASD-associated genes (ASD185) and 664 NDD-associated genes (NDD664) at
477 reduced stringency (FDR $\leq$ 0.05) [38]. For epilepsy-related genes, we used genes categorized
478 by the Epi25 Collaborative (http://epi-25.org/genes-in-epilepsy) and reported by Chen and
479 colleagues [42] that consists of 83 genes identified at p $\leq$ 0.005 by whole-exome sequencing
480 (case-control study) in the full epilepsy cohort (EPI). We next assessed whether expression of

481 ASD-, NDD- and epilepsy-associated genes is regulated in *TSC2*-Null NPCs as determined
482 by anota2seq analysis (i.e. from Figure 3A). This analysis revealed significant enrichments of
483 ASD72 (~43% of all ASD72 genes; $p = 1.72x10^{-7}$) and NDD373 (~37% of all NDD373 genes;
484 $p = 2.59x10^{-19}$) genes among translationally suppressed transcripts as compared to
485 background (Table 1). This finding was further substantiated by applying two approaches that
486 do not use thresholds to identify sets of differentially regulated genes: i) gene set enrichment
487 analysis (GSEA) [41] (Figure 4A) and ii) the same method as applied for *TSC1* vs *TSC2* (i.e.
488 Figure 3D) gene subset-comparisons (Figure 4B, top). Both these approaches showed strong
489 enrichment of ASD72 and NDD373 genes among transcripts translationally suppressed in
490 *TSC2*-Null as compared to isogenic WT NPCs. Similarly, in *TSC2*-Null NPCs, strong
491 enrichments among translationally suppressed genes were observed for the larger ASD185
492 and NDD664 gene sets (Table S2A; Figure S3A, B). ASD- and NDD-associated genes were
493 also enriched among transcripts that were translationally suppressed in both *TSC2*-Null and
494 *TSC1*-Null NPCs relative to their respective controls (i.e. genes from Figure 3E; Table S2B).
495 A similar analysis for EPI-associated genes revealed a smaller enrichment (~27% of all EPI-
496 associated genes; $p = 5.82x10^{-3}$) (Table 1) that was not confirmed using methods that do not
497 use thresholds to identify regulated sets of genes (Figure S3C, D).

498 To assess whether this unexpected translational suppression of ASD- and NDD-
499 associated genes in NPCs occurs in the presence of expected effects on mRNA translation
500 from mTORC1 activation, we applied the same approaches described above to sets of
501 transcripts whose translation was altered following overexpression of eIF4E [39]. Consistent with
502 activation of the mTORC1-eIF4F axis controlling translation in *TSC2*-Null NPCs, there was a
503 strong overlap between genes whose translation was activated upon eIF4E-overexpression
504 and *TSC2* loss (Table S3). A similar result was obtained when only considering genes that
505 were identified as translationally regulated by anota2seq following both *TSC1* and *TSC2* loss
506 (i.e. from Figure 3E; Table S3) and when a method not relying on thresholds was used (Figure
507 4B, middle) as well as when using an additional signature of mTORC1-sensitive translation

508 reported previously [14] (Figure 4B, bottom). Therefore, interestingly, genes associated with
509 ASD and NDD are largely translationally suppressed in NPCs following inactivation of *TSC2*
510 despite appropriate activation of mTORC1-sensitive translation.
511
512 ***5'UTRs of ASD and NDD genes resemble those of mRNAs whose translation is***
513 ***suppressed upon activation of mTORC1***
514 The above results unveiled that translation of mRNAs encoding proteins associated with
515 ASD and NDD is affected by the activity of mTORC1. As mTORC1-sensitive translation largely
516 relies on features in the 5'UTR, this suggests that the observed suppressed translation of
517 ASD- and NDD-associated genes may depend on their 5'UTRs. As mentioned above, mRNAs
518 whose translation parallels activity of mTORC1 often have short and/or highly structured
519 5'UTRs and lack upstream open reading frames (uORFs). Strikingly, ASD- and NDD-
520 associated genes showed an opposite profile for 5'UTR length, GC-content (which associates
521 with secondary structures of the 5'UTR) and uORFs that was more similar to mRNAs whose
522 translation was suppressed upon *TSC2* loss (Figure 4C-E). Therefore, ASD- and NDD-
523 associated genes largely show 5'UTRs that are consistent with translational suppression
524 following increased activation of mTORC1.
525
526 ***RMC-6272 and eFT-508 treatment reverses* TSC2*-dependent translation and***
527 ***encompasses ASD- and NDD-associated genes***
528 The findings above suggest that suppressed translation of ASD- and NDD-associated
529 genes following loss of *TSC2* may be important for neurodevelopmental manifestations.
530 Furthermore, this raises the possibility that inhibition of mTORC1 signaling, or potentially other
531 key pathways modulating translation, may reverse *TSC2*-dependent translation of ASD- and
532 NDD-associated genes. To assess this, we performed polysome-profiling in *TSC2*-Null NPCs
533 treated with mTORC1 inhibitor RMC-6272, or the MNK1/2 inhibitor eFT-508. The resulting
534 dataset was analyzed as described above using anota2seq to determine how these agents

535 modulate gene expression. Both treatments resulted in dramatic mRNA translation changes
536 as visualized in scatterplots comparing effects in polysome-associated and total mRNA levels
537 as well as p-value and FDR densities (Figure S4A-D). Next, we generated gene signatures of
538 transcripts that were translationally increased or decreased in *TSC2*-Null NPCs treated with
539 RMC-6272 relative to DMSO control and determined how these gene sets were regulated in
540 *TSC2*-Null NPCs treated with eFT-508 vs DMSO control. This revealed that transcripts whose
541 translation was activated or suppressed by RMC-6272 showed similar regulation upon eFT-
542 508 treatment and, vice versa, transcripts whose translation was activated or suppressed by
543 eFT-508 showed similar regulation upon RMC-6272 treatment (Figure 5A, B). Yet, these
544 overlaps were partial as subsets of transcripts that were altered in one treatment group did
545 not shift in the other treatment group (Fig. 5A and B). To determine whether the agents
546 reversed *TSC2*-sensitive translation, we used the same strategy as above when comparing
547 *TSC1*- vs *TSC2*-sensitive translation (i.e. Figure 3D). This revealed that both RMC-6272 as
548 well as eFT-508 partially reversed *TSC2*-sensitive translation (Figure 5C). Gene ontology
549 analysis of genes overlapping in *TSC2*-Null NPCs treated with RMC-6272 or eFT-508
550 revealed significant reversal of some cellular functions that were identified as *TSC2*-
551 dependent (shown in Figure 3C), including positive regulation of transcription by RNA
552 polymerase II, positive regulation of RNA metabolic process and protein DNA complex
553 organization along with transcripts involved in various metabolic processes (Figure 5D).

554 By comparing anota2seq outputs for these analyses, we observed that among all
555 transcripts whose translation was increased in *TSC2*-Null cells (Figure 3A), 614 (~47%) or
556 936 (~71%) were suppressed upon RMC-6272 or eFT-508 treatment, respectively, with an
557 overlap of 513 transcripts. Similarly, among all transcripts whose translation was decreased
558 in *TSC2*-Null cells, 1454 (~57%) or 1177 (~46%) were translationally activated upon RMC-
559 6272 or eFT-508 treatment, respectively, with an overlap of 874 transcripts (all overlaps were
560 statistically significant; Figure S4E; Table S4). Gene ontology analyses of *TSC2*-associated
561 changes in translation (from Fig. 3A) that were distinctly reversed upon treatment with either

562 RMC-6272 or eFT-508 revealed significant reversal of enriched annotations upon treatment
563 with RMC-6272 or eFT-508 as well as reversal of key cellular functions shown in Figure 3C
564 (Figure S4F, G).

565 Although the inhibitors led to altered translation of similar numbers of transcripts in *TSC2*-
566 Null NPCs, anota2seq analysis contrasting the two treatments revealed notable differences in
567 terms of affected mRNAs (Figure S5A, B). This was further substantiated by gene ontology
568 analyses, which revealed that while RMC-6272 more efficiently suppressed translation of
569 mRNAs encoding proteins involved in translation and oxidative phosphorylation, eFT-508
570 more efficiently suppressed translation of mRNAs relating to neuronal development (Figure
571 S5C).

572 Next, we assessed whether translation of mRNAs encoding ASD- and NDD-associated
573 genes were affected by mTORC1 and/or MNK1/2 inhibition. This revealed a striking reversal
574 in translation of both ASD and NDD genes in *TSC2*-Null NPCs treated with RMC-6272 or eFT-
575 508 (Figure 6A). To identify affected genes, we compared outputs from the corresponding
576 anota2seq analyses. Among the 31 ASD72 genes translationally suppressed in *TSC2*-Null
577 NPCs, 28 (~90%) and 18 (~58%) were translationally activated upon RMC-6272 (RMC-
578 responsive) and eFT-508 treatment (eFT-responsive), respectively. While all eFT-responsive
579 genes were identified as RMC-responsive, 10 genes were only responsive to RMC-6272
580 (Table 1; Figure 6B). Moreover, for translationally suppressed NDD373 genes, 96 (~70%) and
581 69 (50%) were RMC- and eFT-responsive (Table 1), respectively (60 were both RMC- and
582 eFT-responsive; similar results were obtained for ASD185 and NDD664 genes; Table S2A).
583 To validate alterations in translation upon *TSC2* loss as well as the reversal following mTORC1
584 or MNK1/2 inhibition, we selected five representative ASD/NDD-associated genes that were
585 translationally suppressed in *TSC2*-Null NPCs: *SETD1B* [MIM: 611055], *DYRK1A* [MIM:
586 600855], *CHD8* [MIM: 610528], *NRXN1* [MIM: 600565] and *TCF7L2* [MIM: 62228], and also
587 five eIF4E-sensitive genes that were translationally activated in *TSC2*-Null NPCs: *AP2S1*
588 [MIM: 602242], *LZTR1* [MIM: 600574], *WDR54*, *ALDOC* [MIM: 103870] and *EIF2B2* [MIM:

589 606454]. Quantitative RT-PCR (RT-qPCR) analysis from polysome-associated mRNA
590 fractions (>2 ribosomes), adjusted for alterations in total mRNA, normalized to housekeeping
591 gene, *ACTB* showed a reduction for all five ASD/NDD-related genes and increase in all five
592 eIF4E-sensitive genes in *TSC2*-Null vs WT NPCs, confirming the above polysome-profiling
593 results. Moreover, RMC-6272 or eFT-508 reversed *TSC2*-associated translationally
594 suppressed ASD/NDD and translationally activated eIF4E-sensitive genes (Figure 6C).
595 Similar results were obtained when normalized to a second housekeeping gene *PGK1* (data
596 not shown).

597 Taken together, *TSC2*-dependent decreased translation of mRNAs associated with ASD
598 and NDD can be reversed upon RMC-6272 or eFT-508 treatment in NPCs. These results are
599 intriguing and potentially imply paradoxically suppressed translation of a subset of
600 neurodevelopmentally important genes that nonetheless depend on mTORC1-eIF4F pathway
601 activation.

602

603 **DISCUSSION**

604 The central role of mTORC1 signaling in translation initiation and protein synthesis in a
605 variety of cell types including stem cells, as well as in human disease, is well established [11; 50;
606 51]. While many transcriptome-wide studies have been reported in *TSC1/2*-deficient neuronal
607 cells, how *TSC2* loss affects mRNA translation, particularly in patient-derived cells, is
608 unknown. We recently reported *TSC1*-dependent alterations in mRNA translation employing
609 an isogenic set of CRISPR-modified, TSC1 patient-derived NPCs. Although polysome-
610 profiling revealed a partial reversal of *TSC1*-associated gene expression changes following
611 rapamycin treatment, most genes related to neural activity/synaptic regulation or ASD
612 remained rapamycin-insensitive [25]. Here, we describe generation and characterization of an
613 independent isogenic set of CRISPR-modified NPCs from a TSC patient with a loss-of-function
614 germline mutation in *TSC2*. We find that *TSC2*-Null NPCs mimic *TSC1* loss in activation of
615 mTORC1 signaling and early neurodevelopmental phenotypic changes [25]. Rapamycin

616 treatment of *TSC2*-Null NPCs fully inhibited phosphorylation of S6K and reduced enlarged cell
617 size but had minimal effects on 4E-BP1 phosphorylation and early neurodevelopmental
618 phenotypes. In contrast, the third-generation mTORC1 inhibitor RMC-6272 revealed efficient
619 inhibition of both S6K and 4E-BP1 phosphorylation and rescued these phenotypes as well as
620 cell size. These data suggest that while enlarged cell size observed upon *TSC2* loss depends
621 on the mTORC1-S6K axis of the pathway, which is consistent with previous reports [47], the
622 altered neurodevelopmental phenotypes depend on the mTORC1-4E-BP1 signaling axis.
623 We observed dramatic changes in mRNA translation associated with *TSC2* loss in NPCs
624 that largely overlapped with those observed upon *TSC1* loss. Provided that *TSC1* and *TSC2*
625 loss-assert similar effects on mTORC1 signaling, a substantial overlap is expected. Importantly
626 as the cells were derived from independent patients, our results support a robust effect on
627 mRNA translation across patients with hyperactive mTORC1 activity. In this study, in addition
628 to RMC-6272, which inhibits mTORC1 activity, we also considered alternative approaches to
629 modulate activity of the eIF4F complex and therefore included the MNK1/2 inhibitor eFT-
630 508/tomivosertib to understand a possible convergence of mTORC1-4E-BP1 and MNK-eIF4E
631 signaling pathways on *TSC2*-dependent protein synthesis (see Figure 1A). While mTORC1-
632 sensitive translation has been studied extensively at the transcriptome-wide level [22; 40; 52; 53],
633 the understanding of how the MNK-eIF4E axis modulates mRNA translation at a global scale
634 is more limited [16]. This study is the first that includes a direct comparison of these pathways
635 to assess effects on mRNA translation at a transcriptome-wide level, and the results reveal
636 that a large proportion of translational alterations observed in *TSC2*-Null NPCs can be
637 reversed by RMC-6272 or eFT-508, suggesting that these changes are mediated by
638 mTORC1-4E-BP1- and MNK-eIF4E-dependent activation of eIF4F complex. However, the
639 activity of the two inhibitors is not equivalent since RMC-6272 would be expected to affect
640 both eIF4E-dependent and S6K-dependent translation whereas eFT-508 would be restricted
641 to MNK1/2-dependent translation. We also observe ample differences between the two drugs
642 with respect to translation, which are in line with previous studies showing differences in

643 affected cellular phenotypes as the mTORC1-4E-BP1 axis is a key regulator of cell cycle
644 progression [19; 54] while MNK1/2-eIF4E controls cell migration [55; 56].
645 As epilepsy and ASD are strongly associated with TSC, we compared transcripts that were
646 differentially translated in *TSC2*-Null vs WT NPCs to recent genetic datasets available from
647 large cohorts of individuals with ASD, NDD and epilepsy [38; 42]. Interestingly, numerous non-
648 monogenic ASD-, NDD- and epilepsy-associated genes identified in patients harboring
649 putative loss-of-function mutations, including protein truncating or damaging missense
650 variants, were translationally suppressed in *TSC2*-Null NPCs and overlapped with data from
651 our previously reported *TSC1*-model. Notably, the results for ASD- and NDD-associated
652 genes were confirmed using multiple methods, which suggests that for these subsets there is
653 a strong negative regulatory effect on mRNA translation impacting a large proportion of these
654 mRNAs. This was not the case for epilepsy-associated genes, in that a smaller fraction of
655 these genes was translationally suppressed upon *TSC2* loss. Importantly, these decreases in
656 translation were observed side-by-side with the expected increased translation of mRNAs that
657 were previously reported to be translationally activated upon mTORC1 pathway activation.
658 This suppressed translation was, for a majority of identified ASD/NDD genes, reversed by
659 inhibition of mTORC1 using RMC-6272 or MNK1/2 using eFT-508. A recent elegant large-
660 scale transcriptome study demonstrated that CRISPR perturbation of several ASD genes
661 results in differential expression of ASD/NDD-related genes that positively correlate with co-
662 expression of the perturbed gene, thereby establishing a high level of convergence across
663 ASD risk genes [57]. Our results here showing translational suppression of many ASD/NDD
664 genes upon loss of *TSC2* is consistent with the positive correlation and co-expression reported
665 by Liao and colleagues [57]. However, most notably, our results demonstrate that a majority of
666 translationally suppressed ASD/NDD/epilepsy genes can be reversed by RMC-6272 or eFT-
667 508, thereby establishing the roles of mTORC1-4E-BP1 and MNK-eIF4E in regulating
668 translation of these genes.

669 Many of the translationally suppressed ASD genes are FMRP targets. FMRP was
670 originally considered to function as a translational repressor that can bind to numerous mRNAs
671 that are generally larger than average and enriched for genes associated with ID and ASD [58;
672 59]. However, recent studies of FMRP-deficiency have documented a decrease in translation
673 initiation rates of many FMRP targets including ASD-related genes, which contrasts the notion
674 that FMRP is solely a translational repressor and supports a model where FMRP can also
675 function to increase the translation initiation of many targets [60-63]. Furthermore, in *TSC2*-Null
676 NPCs we also observe that 32 translationally suppressed ASD/NDD-related genes are
677 associated with chromatin-remodeling [64; 65]. Additional studies are therefore necessary to fully
678 comprehend how the ASD- and NDD-associated genes are translationally suppressed upon
679 loss of *TSC2*.

680 In the literature, the focus has been, in general, towards understanding mechanisms
681 underlying transcript-selective translation paralleling mTORC1 activity [13] while less attention
682 has been given to transcript that show decreased translation upon mTORC1 activation.
683 Translation of mRNAs enriched for 5'UTRs containing uORFs are translationally suppressed
684 upon mTORC1 activation [40]. In agreement, we observed an increased frequency of uORFs in
685 both ASD- and NDD-associated genes; however, it should be noted that uORFs are also
686 common among background transcripts, and a relatively large proportion of ASD- and NDD-
687 associated genes do not have uORFs in their 5'UTRs.

688 Our results raise the critical question as to how ASD/NDD-related genes are translationally
689 suppressed upon mTORC1 activation in *TSC2*-Null NPCs. In addition to mTORC1 signaling,
690 the integrated stress response (ISR) pathway, which selectively modulates translation of
691 transcripts with 5'UTRs harboring uORFs [66], is a key regulator of mRNA translation. In
692 response to cellular stress, a decrease in global protein synthesis is paralleled by increased
693 translation of mRNAs with 5'-uORFs including the transcription factor ATF4 (reviewed in [67]);
694 therefore, further studies are need to examine involvement of the ISR pathway in our TSC

695 models. Furthermore, alternative mechanisms such as DAP5-dependent translation, which
696 can be activated under low mTORC1 signaling, may also play a role [53].
697 Another potential mechanism of translational regulation is via microRNAs (miRNAs), which
698 are involved in neurodevelopmental disorders [68]. Among 31 translationally suppressed
699 transcripts in *TSC2*-Null NPCs that show strong association with ASD (ASD72, FDR<0.001),
700 28 are predicted to be targeted by at least one miRNA, using the miTarBase 2017 library (data
701 not shown). Interestingly, of the individual miRNAs identified by miTarBase analysis, four (hsa-
702 miR-27b-3p, hsa-let-7g-3p, hsa-miR-29a-3p and hsa-miR-515-5p) were reported as increased
703 upon *TSC1*- or *TSC2*-shRNA suppression in human neural stem cells generated from skin
704 fibroblast-derived iPSCs ($p < 0.05$) [69]; and three (hsa-miR-21-5p, hsa-miR-19b-3p and hsa-
705 miR-144-3p) were shown to be overexpressed in human autism brain samples [70]. Based on
706 this, it is tempting to speculate that miRNAs may play a role in suppressing translation in
707 *TSC2*-Null NPCs, and future studies will address this mechanistic possibility.
708 In summary, we establish that loss of *TSC2* in patient-derived NPCs results in numerous
709 changes in mRNA translation, which significantly overlap with loss of *TSC1*. Loss of *TSC2*
710 associates with suppressed translation of a large proportion of ASD- and NDD-related genes,
711 which is reversed by inhibition of mTORC1 or MNK1/2, demonstrating the importance of
712 eIF4F-dependent mRNA translation in neurodevelopmental disorders. Our work also supports
713 the therapeutic potential for RMC-5552 (the clinical counterpart of RMC-6272) and eFT-
714 508/tomivosertib that are currently under clinical development for cancer, as a strategy for
715 treatment of TSC-associated neuropsychiatric disorders as well as ASD and other
716 neurodevelopmental disorders.
717
718 **DECLARATION OF INTERESTS**
719 The authors declare no competing interests.
720
721 **ACKNOWLEDGEMENTS**

This paper is dedicated to the memory of the late Dr. Jerry Pelletier, a distinguished James McGill Professor in the Department of Biochemistry and Oncology from the Goodman Cancer Institute at McGill University, Montreal, Canada, who unfortunately passed away during the completion of this study. This work was supported by NIH R01 NS109540 (V.R.), the Swedish Brain foundation FO2022-0178 (O.L.); the Swedish research council 2020-01665 (O.L.); the Wallenberg academy fellow program 2013.0181 (O.L.). We thank Revolution Medicines, Inc. for generously providing RMC-6272 for this study. Our sincere thanks to Dr. Justin Meyerowitz and Dr. Mallika Singh of Revolution Medicines, Inc. for their valuable comments on the manuscript.

AUTHOR CONTRIBUTIONS

Conceptualization and study design: V.R. and O.L.; experimental methods and data acquisition P.M., K.S., F.R., S.B., R.B., N.R., J.B., S.C. and I.N.; data analysis and interpretation: P.M., K.S., F.R., S.B., R.B. S.C., I.N., S.H., S.E. and O.L.; manuscript preparation and editing: P.M., K.S., F.R., S.B., R.B., I.N., S.H., S.E., O.L. and V.R.

WEB RESOURCES

OMIM, https://www.omim.org/

NCBI GenBank, https://www.ncbi.nlm.nih.gov/genbank/

Sequences,https://www.ncbi.nlm.nih.gov/nuccore/NM_000548

GenScript, https://www.genscript.com

BBTools software suite, https://www.osti.gov/servlets/purl/1241166

fgsea package (v.1.24.0), https://doi.org/10.18129/B9.bioc.fgsea

R statistical software environment, https://www.R-project.org/

DATA AND CODE AVAILABILITY

748 The polysome-profiling datasets supporting the conclusions of this article are included
749 within the article (and its additional file(s)), and the full datasets will be deposited into Gene
750 Expression Omnibus (GEO).
751
752
753 **REFERENCES**

754 1. de Vries, P.J., Heunis, T.M., Vanclooster, S., Chambers, N., Bissell, S., Byars, A.W., Flinn,
755 J., Gipson, T.T., van Eeghen, A.M., Waltereit, R., et al. (2023). International consensus
756 recommendations for the identification and treatment of tuberous sclerosis complex-
757 associated neuropsychiatric disorders (TAND). J Neurodev Disord 15, 32.
758 2. Henske, E.P., Jozwiak, S., Kingswood, J.C., Sampson, J.R., and Thiele, E.A. (2016).
759 Tuberous sclerosis complex. Nat Rev Dis Primers 2, 16035.
760 3. Sahin, M., Henske, E.P., Manning, B.D., Ess, K.C., Bissler, J.J., Klann, E., Kwiatkowski,
761 D.J., Roberds, S.L., Silva, A.J., Hillaire-Clarke, C.S., et al. (2016). Advances and
762 Future Directions for Tuberous Sclerosis Complex Research: Recommendations From
763 the 2015 Strategic Planning Conference. Pediatr Neurol 60, 1-12.
764 4. Bissler, J.J., McCormack, F.X., Young, L.R., Elwing, J.M., Chuck, G., Leonard, J.M.,
765 Schmithorst, V.J., Laor, T., Brody, A.S., Bean, J., et al. (2008). Sirolimus for
766 angiomyolipoma in tuberous sclerosis complex or lymphangioleiomyomatosis. N Engl
767 J Med 358, 140-151.
768 5. Davies, D.M., de Vries, P.J., Johnson, S.R., McCartney, D.L., Cox, J.A., Serra, A.L.,
769 Watson, P.C., Howe, C.J., Doyle, T., Pointon, K., et al. (2011). Sirolimus therapy for
770 angiomyolipoma in tuberous sclerosis and sporadic lymphangioleiomyomatosis: a
771 phase 2 trial. Clinical cancer research : an official journal of the American Association
772 for Cancer Research 17, 4071-4081.
773 6. Julich, K., and Sahin, M. (2014). Mechanism-based treatment in tuberous sclerosis
774 complex. Pediatric neurology 50, 290-296.

775 7. Krueger, D.A., Care, M.M., Holland, K., Agricola, K., Tudor, C., Mangeshkar, P., Wilson,
776 K.A., Byars, A., Sahmoud, T., and Franz, D.N. (2010). Everolimus for subependymal
777 giant-cell astrocytomas in tuberous sclerosis. The New England journal of medicine
778 363, 1801-1811.
779 8. Overwater, I.E., Rietman, A.B., van Eeghen, A.M., and de Wit, M.C.Y. (2019). Everolimus
780 for the treatment of refractory seizures associated with tuberous sclerosis complex
781 (TSC): current perspectives. Ther Clin Risk Manag 15, 951-955.
782 9. Krueger, D.A., Sadhwani, A., Byars, A.W., de Vries, P.J., Franz, D.N., Whittemore, V.H.,
783 Filip-Dhima, R., Murray, D., Kapur, K., and Sahin, M. (2017). Everolimus for treatment
784 of tuberous sclerosis complex-associated neuropsychiatric disorders. Ann Clin Transl
785 Neurol 4, 877-887.
786 10. Overwater, I.E., Rietman, A.B., Mous, S.E., Bindels-de Heus, K., Rizopoulos, D., Ten
787 Hoopen, L.W., van der Vaart, T., Jansen, F.E., Elgersma, Y., Moll, H.A., et al. (2019).
788 A randomized controlled trial with everolimus for IQ and autism in tuberous sclerosis
789 complex. Neurology 93, e200-e209.
790 11. Saba, J.A., Liakath-Ali, K., Green, R., and Watt, F.M. (2021). Translational control of stem
791 cell function. Nat Rev Mol Cell Biol 22, 671-690.
792 12. Thoreen, C.C. (2017). The molecular basis of mTORC1-regulated translation. Biochem
793 Soc Trans 45, 213-221.
794 13. Masvidal, L., Hulea, L., Furic, L., Topisirovic, I., and Larsson, O. (2017). mTOR-sensitive
795 translation: Cleared fog reveals more trees. RNA Biol 14, 1299-1305.
796 14. Gandin, V., Masvidal, L., Cargnello, M., Gyenis, L., McLaughlan, S., Cai, Y., Tenkerian,
797 C., Morita, M., Balanathan, P., Jean-Jean, O., et al. (2016). mTORC1 and CK2
798 coordinate ternary and eIF4F complex assembly. Nat Commun 7, 11127.
799 15. Bramham, C.R., Jensen, K.B., and Proud, C.G. (2016). Tuning Specific Translation in
800 Cancer Metastasis and Synaptic Memory: Control at the MNK-eIF4E Axis. Trends
801 Biochem Sci 41, 847-858.

802 16. Karampelias, C., Watt, K., Mattsson, C.L., Ruiz, A.F., Rezanejad, H., Mi, J., Liu, X., Chu,
803 L., Locasale, J.W., Korbutt, G.S., et al. (2022). MNK2 deficiency potentiates beta-cell
804 regeneration via translational regulation. Nat Chem Biol 18, 942-953.
805 17. Choo, A.Y., Yoon, S.O., Kim, S.G., Roux, P.P., and Blenis, J. (2008). Rapamycin
806 differentially inhibits S6Ks and 4E-BP1 to mediate cell-type-specific repression of
807 mRNA translation. Proceedings of the National Academy of Sciences of the United
808 States of America 105, 17414-17419.
809 18. Fan, Q.W., Nicolaides, T.P., and Weiss, W.A. (2018). Inhibiting 4EBP1 in Glioblastoma.
810 Clin Cancer Res 24, 14-21.
811 19. Larsson, O., Morita, M., Topisirovic, I., Alain, T., Blouin, M.J., Pollak, M., and Sonenberg,
812 N. (2012). Distinct perturbation of the translatome by the antidiabetic drug metformin.
813 Proc Natl Acad Sci U S A 109, 8977-8982.
814 20. Rodrik-Outmezguine, V.S., Okaniwa, M., Yao, Z., Novotny, C.J., McWhirter, C., Banaji, A.,
815 Won, H., Wong, W., Berger, M., de Stanchina, E., et al. (2016). Overcoming mTOR
816 resistance mutations with a new-generation mTOR inhibitor. Nature 534, 272-276.
817 21. Burnett, G.L., Yang, Y.C., Aggen, J.B., Pitzen, J., Gliedt, M.K., Semko, C.M., Marquez, A.,
818 Evans, J.W., Wang, G., Won, W.S., et al. (2023). Discovery of RMC-5552, a Selective
819 Bi-Steric Inhibitor of mTORC1, for the Treatment of mTORC1-Activated Tumors. J Med
820 Chem 66, 149-169.
821 22. Lee, B.J., Boyer, J.A., Burnett, G.L., Thottumkara, A.P., Tibrewal, N., Wilson, S.L., Hsieh,
822 T., Marquez, A., Lorenzana, E.G., Evans, J.W., et al. (2021). Selective inhibitors of
823 mTORC1 activate 4EBP1 and suppress tumor growth. Nat Chem Biol 17, 1065-1074.
824 23. Bhattacharyya, S., Oblinger, J.L., Beauchamp, R.L., Kosa, L., Robert, F., Plotkin, S.R.,
825 Chang, L.S., and Ramesh, V. (2024). Preclinical evaluation of the third-generation, bi-
826 steric mechanistic target of rapamycin complex 1-selective inhibitor RMC-6272 in NF2-
827 deficient models. Neurooncol Adv 6, vdae024.

828 24. Reich, S.H., Sprengeler, P.A., Chiang, G.G., Appleman, J.R., Chen, J., Clarine, J., Eam,
829 B., Ernst, J.T., Han, Q., Goel, V.K., et al. (2018). Structure-based Design of Pyridone-
830 Aminal eFT508 Targeting Dysregulated Translation by Selective Mitogen-activated
831 Protein Kinase Interacting Kinases 1 and 2 (MNK1/2) Inhibition. J Med Chem 61, 3516-
832 3540.
833 25. Aksoylu, I.S., Martin, P., Robert, F., Szkop, K.J., Redmond, N.E., Bhattacharyya, S.,
834 Wang, J., Chen, S., Beauchamp, R.L., Nobeli, I., et al. (2023). Translatome analysis
835 of tuberous sclerosis complex 1 patient-derived neural progenitor cells reveals
836 rapamycin-dependent and independent alterations. Mol Autism 14, 39.
837 26. Niida, Y., Stemmer-Rachamimov, A.O., Logrip, M., Tapon, D., Perez, R., Kwiatkowski,
838 D.J., Sims, K., MacCollin, M., Louis, D.N., and Ramesh, V. (2001). Survey of somatic
839 mutations in tuberous sclerosis complex (TSC) hamartomas suggests different genetic
840 mechanisms for pathogenesis of TSC lesions. Am J Hum Genet 69, 493-503.
841 27. Schlaeger, T.M., Daheron, L., Brickler, T.R., Entwisle, S., Chan, K., Cianci, A., DeVine, A.,
842 Ettenger, A., Fitzgerald, K., Godfrey, M., et al. (2015). A comparison of non-integrating
843 reprogramming methods. Nat Biotechnol 33, 58-63.
844 28. Warren, L., Manos, P.D., Ahfeldt, T., Loh, Y.H., Li, H., Lau, F., Ebina, W., Mandal, P.K.,
845 Smith, Z.D., Meissner, A., et al. (2010). Highly efficient reprogramming to pluripotency
846 and directed differentiation of human cells with synthetic modified mRNA. Cell Stem
847 Cell 7, 618-630.
848 29. Martin, P., Wagh, V., Reis, S.A., Erdin, S., Beauchamp, R.L., Shaikh, G., Talkowski, M.,
849 Thiele, E., Sheridan, S.D., Haggarty, S.J., et al. (2020). TSC patient-derived isogenic
850 neural progenitor cells reveal altered early neurodevelopmental phenotypes and
851 rapamycin-induced MNK-eIF4E signaling. Mol Autism 11, 2.
852 30. Sellgren, C.M., Gracias, J., Watmuff, B., Biag, J.D., Thanos, J.M., Whittredge, P.B., Fu,
853 T., Worringer, K., Brown, H.E., Wang, J., et al. (2019). Increased synapse elimination

854 by microglia in schizophrenia patient-derived models of synaptic pruning. Nat Neurosci
855 22, 374-385.
856 31. Han, S., Kim, S., Bahl, S., Li, L., Burande, C.F., Smith, N., James, M., Beauchamp, R.L.,
857 Bhide, P., Diantonio, A., et al. (2012). The E3 Ubiquitin Ligase Protein Associated with
858 Myc (Pam) Regulates Mammalian/Mechanistic Target of Rapamycin Complex 1
859 (mTORC1) Signaling in Vivo through N- and C-terminal Domains. The Journal of
860 biological chemistry 287, 30063-30072.
861 32. James, M.F., Han, S., Polizzano, C., Plotkin, S.R., Manning, B.D., Stemmer-Rachamimov,
862 A.O., Gusella, J.F., and Ramesh, V. (2009). NF2/merlin is a novel negative regulator
863 of mTOR complex 1, and activation of mTORC1 is associated with meningioma and
864 schwannoma growth. Molecular and cellular biology 29, 4250-4261.
865 33. Wang, D., Lagerstrom, R., Sun, C., Bishof, L., Valotton, P., and Gotte, M. (2010). HCA-
866 vision: Automated neurite outgrowth analysis. J Biomol Screen 15, 1165-1170.
867 34. Gandin, V., Sikstrom, K., Alain, T., Morita, M., McLaughlan, S., Larsson, O., and
868 Topisirovic, I. (2014). Polysome fractionation and analysis of mammalian translatomes
869 on a genome-wide scale. J Vis Exp.
870 35. Kim, D., Paggi, J.M., Park, C., Bennett, C., and Salzberg, S.L. (2019). Graph-based
871 genome alignment and genotyping with HISAT2 and HISAT-genotype. Nat Biotechnol
872 37, 907-915.
873 36. Liao, Y., Smyth, G.K., and Shi, W. (2019). The R package Rsubread is easier, faster,
874 cheaper and better for alignment and quantification of RNA sequencing reads. Nucleic
875 Acids Res 47, e47.
876 37. Oertlin, C., Lorent, J., Murie, C., Furic, L., Topisirovic, I., and Larsson, O. (2019). Generally
877 applicable transcriptome-wide analysis of translation using anota2seq. Nucleic Acids
878 Res 47, e70.

879 38. Fu, J.M., Satterstrom, F.K., Peng, M., Brand, H., Collins, R.L., Dong, S., Wamsley, B., Klei,
880 L., Wang, L., Hao, S.P., et al. (2022). Rare coding variation provides insight into the
881 genetic architecture and phenotypic context of autism. Nat Genet 54, 1320-1331.
882 39. Larsson, O., Li, S., Issaenko, O.A., Avdulov, S., Peterson, M., Smith, K., Bitterman, P.B.,
883 and Polunovsky, V.A. (2007). Eukaryotic translation initiation factor 4E induced
884 progression of primary human mammary epithelial cells along the cancer pathway is
885 associated with targeted translational deregulation of oncogenic drivers and inhibitors.
886 Cancer Res 67, 6814-6824.
887 40. Gandin, V., Masvidal, L., Hulea, L., Gravel, S.P., Cargnello, M., McLaughlan, S., Cai, Y.,
888 Balanathan, P., Morita, M., Rajakumar, A., et al. (2016). nanoCAGE reveals 5' UTR
889 features that define specific modes of translation of functionally related MTOR-
890 sensitive mRNAs. Genome Res 26, 636-648.
891 41. Subramanian, A., Tamayo, P., Mootha, V.K., Mukherjee, S., Ebert, B.L., Gillette, M.A.,
892 Paulovich, A., Pomeroy, S.L., Golub, T.R., Lander, E.S., et al. (2005). Gene set
893 enrichment analysis: a knowledge-based approach for interpreting genome-wide
894 expression profiles. Proc Natl Acad Sci U S A 102, 15545-15550.
895 42. Chen, S., Neale, B.M., and Berkovic, S.F. (2023). Shared and distinct ultra-rare genetic
896 risk for diverse epilepsies: A whole-exome sequencing study of 54,423 individuals
897 across multiple genetic ancestries. medRxiv, doi: 10.1101/2023.02.22.23286310.
898 43. Blair, J.D., Hockemeyer, D., and Bateup, H.S. (2018). Genetically engineered human
899 cortical spheroid models of tuberous sclerosis. Nat Med 24, 1568-1578.
900 44. Costa, V., Aigner, S., Vukcevic, M., Sauter, E., Behr, K., Ebeling, M., Dunkley, T., Friedlein,
901 A., Zoffmann, S., Meyer, C.A., et al. (2016). mTORC1 Inhibition Corrects
902 Neurodevelopmental and Synaptic Alterations in a Human Stem Cell Model of
903 Tuberous Sclerosis. Cell Rep 15, 86-95.
904 45. Sundberg, M., Tochitsky, I., Buchholz, D.E., Winden, K., Kujala, V., Kapur, K., Cataltepe,
905 D., Turner, D., Han, M.J., Woolf, C.J., et al. (2018). Purkinje cells derived from TSC

906 patients display hypoexcitability and synaptic deficits associated with reduced FMRP
907 levels and reversed by rapamycin. Mol Psychiatry 23, 2167-2183.
908 46. Zucco, A.J., Pozzo, V.D., Afinogenova, A., Hart, R.P., Devinsky, O., and D'Arcangelo, G.
909 (2018). Neural progenitors derived from Tuberous Sclerosis Complex patients exhibit
910 attenuated PI3K/AKT signaling and delayed neuronal differentiation. Mol Cell Neurosci
911 92, 149-163.
912 47. Dowling, R.J., Topisirovic, I., Alain, T., Bidinosti, M., Fonseca, B.D., Petroulakis, E., Wang,
913 X., Larsson, O., Selvaraj, A., Liu, Y., et al. (2010). mTORC1-mediated cell proliferation,
914 but not cell growth, controlled by the 4E-BPs. Science 328, 1172-1176.
915 48. Oertlin, C., Watt, K., Ristau, J., and Larsson, O. (2022). Anota2seq Analysis for
916 Transcriptome-Wide Studies of mRNA Translation. Methods Mol Biol 2418, 243-268.
917 49. Sandri, B.J., Masvidal, L., Murie, C., Bartish, M., Avdulov, S., Higgins, L., Markowski, T.,
918 Peterson, M., Bergh, J., Yang, P., et al. (2019). Distinct Cancer-Promoting Stromal
919 Gene Expression Depending on Lung Function. Am J Respir Crit Care Med 200, 348-
920 358.
921 50. Bartish, M., Abraham, M.J., Goncalves, C., Larsson, O., Rolny, C., and Del Rincon, S.V.
922 (2023). The role of eIF4F-driven mRNA translation in regulating the tumour
923 microenvironment. Nat Rev Cancer 23, 408-425.
924 51. Tahmasebi, S., Khoutorsky, A., Mathews, M.B., and Sonenberg, N. (2018). Translation
925 deregulation in human disease. Nat Rev Mol Cell Biol 19, 791-807.
926 52. Silvera, D., Ernlund, A., Arju, R., Connolly, E., Volta, V., Wang, J., and Schneider, R.J.
927 (2017). mTORC1 and -2 Coordinate Transcriptional and Translational Reprogramming
928 in Resistance to DNA Damage and Replicative Stress in Breast Cancer Cells. Mol Cell
929 Biol 37.
930 53. Volta, V., Perez-Baos, S., de la Parra, C., Katsara, O., Ernlund, A., Dornbaum, S., and
931 Schneider, R.J. (2021). A DAP5/eIF3d alternate mRNA translation mechanism

932 promotes differentiation and immune suppression by human regulatory T cells. Nat
933 Commun 12, 6979.
934 54. Mamane, Y., Petroulakis, E., Martineau, Y., Sato, T.A., Larsson, O., Rajasekhar, V.K., and
935 Sonenberg, N. (2007). Epigenetic activation of a subset of mRNAs by eIF4E explains
936 its effects on cell proliferation. PLoS One 2, e242.
937 55. Beggs, J.E., Tian, S., Jones, G.G., Xie, J., Iadevaia, V., Jenei, V., Thomas, G., and Proud,
938 C.G. (2015). The MAP kinase-interacting kinases regulate cell migration, vimentin
939 expression and eIF4E/CYFIP1 binding. Biochem J 467, 63-76.
940 56. Robichaud, N., del Rincon, S.V., Huor, B., Alain, T., Petruccelli, L.A., Hearnden, J.,
941 Goncalves, C., Grotegut, S., Spruck, C.H., Furic, L., et al. (2015). Phosphorylation of
942 eIF4E promotes EMT and metastasis via translational control of SNAIL and MMP-3.
943 Oncogene 34, 2032-2042.
944 57. Liao, C., Moyses-Oliveira, M., De Esch, C.E.F., Bhavsar, R., Nuttle, X., Li, A., Yu, A., Burt,
945 N.D., Erdin, S., Fu, J.M., et al. (2023). Convergent coexpression of autism-associated
946 genes suggests some novel risk genes may not be detectable in large-scale genetic
947 studies. Cell Genom 3, 100277.
948 58. Ascano, M., Jr., Mukherjee, N., Bandaru, P., Miller, J.B., Nusbaum, J.D., Corcoran, D.L.,
949 Langlois, C., Munschauer, M., Dewell, S., Hafner, M., et al. (2012). FMRP targets
950 distinct mRNA sequence elements to regulate protein expression. Nature 492, 382-
951 386.
952 59. Darnell, J.C., Van Driesche, S.J., Zhang, C., Hung, K.Y., Mele, A., Fraser, C.E., Stone,
953 E.F., Chen, C., Fak, J.J., Chi, S.W., et al. (2011). FMRP stalls ribosomal translocation
954 on mRNAs linked to synaptic function and autism. Cell 146, 247-261.
955 60. Das Sharma, S., Metz, J.B., Li, H., Hobson, B.D., Hornstein, N., Sulzer, D., Tang, G., and
956 Sims, P.A. (2019). Widespread Alterations in Translation Elongation in the Brain of
957 Juvenile Fmr1 Knockout Mice. Cell Rep 26, 3313-3322 e3315.

958 61. Flanagan, K., Baradaran-Heravi, A., Yin, Q., Dao Duc, K., Spradling, A.C., and Greenblatt,
959 E.J. (2022). FMRP-dependent production of large dosage-sensitive proteins is highly
960 conserved. Genetics 221.
961 62. Richter, J.D., and Zhao, X. (2021). The molecular biology of FMRP: new insights into
962 fragile X syndrome. Nat Rev Neurosci 22, 209-222.
963 63. Sawicka, K., Hale, C.R., Park, C.Y., Fak, J.J., Gresack, J.E., Van Driesche, S.J., Kang,
964 J.J., Darnell, J.C., and Darnell, R.B. (2019). FMRP has a cell-type-specific role in CA1
965 pyramidal neurons to regulate autism-related transcripts and circadian memory. Elife
966 8.
967 64. Gabriele, M., Lopez Tobon, A., D'Agostino, G., and Testa, G. (2018). The chromatin basis
968 of neurodevelopmental disorders: Rethinking dysfunction along the molecular and
969 temporal axes. Prog Neuropsychopharmacol Biol Psychiatry 84, 306-327.
970 65. Mossink, B., Negwer, M., Schubert, D., and Nadif Kasri, N. (2021). The emerging role of
971 chromatin remodelers in neurodevelopmental disorders: a developmental perspective.
972 Cell Mol Life Sci 78, 2517-2563.
973 66. Guan, B.J., van Hoef, V., Jobava, R., Elroy-Stein, O., Valasek, L.S., Cargnello, M., Gao,
974 X.H., Krokowski, D., Merrick, W.C., Kimball, S.R., et al. (2017). A Unique ISR Program
975 Determines Cellular Responses to Chronic Stress. Mol Cell 68, 885-900 e886.
976 67. Pakos-Zebrucka, K., Koryga, I., Mnich, K., Ljujic, M., Samali, A., and Gorman, A.M. (2016).
977 The integrated stress response. EMBO Rep 17, 1374-1395.
978 68. Sun, E., and Shi, Y. (2015). MicroRNAs: Small molecules with big roles in
979 neurodevelopment and diseases. Exp Neurol 268, 46-53.
980 69. Pawlik, B., Grabia, S., Smyczynska, U., Fendler, W., Drozdz, I., Liszewska, E., Jaworski,
981 J., Kotulska, K., Jozwiak, S., Mlynarski, W., et al. (2022). MicroRNA Expression Profile
982 in TSC Cell Lines and the Impact of mTOR Inhibitor. Int J Mol Sci 23.

983 70. Mor, M., Nardone, S., Sams, D.S., and Elliott, E. (2015). Hypomethylation of miR-142
984 promoter and upregulation of microRNAs that target the oxytocin receptor gene in the
985 autism prefrontal cortex. Mol Autism 6, 46.
986

987 **FIGURE TITLES AND LEGENDS**

988

989 **Figure 1. Inhibition of mTORC1 using RMC-6272 or rapamycin rescues increased cell**
990 **size in *TSC2*-mutant NPCs.**
991 (A) Schematic representation of how mTORC1 signaling modulates mRNA translation.
992 Inhibitors used to target the pathway axes are indicated in red.
993 (B) Representative bright field images, including enlarged inset images (black boxed regions),
994 are shown for *TSC2*-Het and -Null NPCs compared with *TSC2*-WT cells. Scale bar=100µm.
995 (C) Immunoblotting of an isogenic set of *TSC2*-WT, -Het and -Null (cl. 39) NPCs, following 24
996 h treatment with DMSO (control), rapamycin (50nM) or RMC-6272 (10nM) are shown for
997 TSC2/tuberin as well as mTORC1 pathway readouts pS6K T389, pS6 S240/244 and p4E-BP1
998 S65 along with respective total proteins.
999 (D) Average cell size for *TSC2*-Het and -Null NPCs relative to *TSC2*-WT cells following a 48
1000 h treatment with DMSO (control), rapamycin or RMC-6272 (same concentrations as in C) was
1001 quantitated, and data represents the mean (±SEM) from 3 independent experiments, each
1002 with triplicate technical replicates. P-values of comparisons (*$p<0.05$, **$p<0.01$, ***$p<0.001$)
1003 from Student's t-test are indicated.
1004

1005 **Figure 2. Altered neurodevelopmental phenotypes in *TSC2* mutant NPCs are rescued**
1006 **by RMC-6272, but not rapamycin.**
1007 (A) Proliferation by live cell counting (trypan blue exclusion) was carried out over days D1-4
1008 in *TSC2*-WT, -Het and -Null NPCs under control treatment (left graph region), or treatment
1009 initiated at D1 with rapamycin (50 nM, middle graph region) or RMC-6272 (10 nM, right graph

1010 region). Quantitation for each timepoint is normalized to cell seeding number (D0=1). Data
1011 represent the mean (±SEM) from 3 independent experiments (3 replicates/cell
1012 line/experiment). Student's t-test p-values (*p<0.05, **p<0.01, ***p<0.001) are indicated in
1013 DMSO-treated NPCs (left graph region) for increasing cell numbers in *TSC2*-Het and Null
1014 NPCs at each timepoint (D1-4) relative to *TSC2*-WT NPCs at the respective timepoint. For
1015 drug-treated NPCs (middle and right graph regions), within each genotype, p-values are
1016 indicated for changes in cell numbers relative to DMSO controls at the corresponding
1017 timepoint.
1018 (B) Representative images of immunofluorescence staining in NPCs using neuronal marker
1019 MAP2 (gray), performed 48 h after initiating nerite outgrowth, are shown along with traced
1020 images generated employing HCA-Vision image quantitation software (green), which traces
1021 the cell body along branching layers of the neurite arborization. Scale bar = 100 µm.
1022 (C and D) Bar plots indicate average neurite length (left panel), average neurite number
1023 (center) and extremities (right) per cell for *TSC2*-Het and -Null NPCs relative to *TSC2*-WT
1024 NPCs under control conditions (C) or for rapamycin (50 nM) or RMC-6272 (10 nM) treatment
1025 in *TSC2*-Het and -Null cells relative to DMSO control (D) . Data represents mean (±SEM) from
1026 3 independent experiments (8 non-overlapping image fields/cell line/experiment). P-values
1027 from Student's t-test (*p<0.05, **p<0.01, ***p<0.001) are shown.
1028
1029 **Figure 3. Extensive remodeling of mRNA translation in *TSC2*-Null NPCs aligns with**
1030 **those observed following loss of *TSC1*.**
1031 (A) Scatterplot of polysome-associated mRNA vs total mRNA log2 fold changes between
1032 *TSC2*-Null (-/-) and WT NPCs. Genes are colored according to their mode of regulation as
1033 identified by the anota2seq analysis (FDR < 0.15). The number of mRNAs regulated via
1034 translation, mRNA abundance or offsetting is indicated.
1035 (B) Kernel densities of p-values and FDRs (from anota2seq analysis) for the comparison of
1036 *TSC2*-Null vs WT NPCs. Densities are shown for analysis of polysome-associated RNA

1037 (translated mRNA), total mRNA, translation and offsetting. A shift of the density towards low
1038 p-values/FDRs indicates a higher frequency of changes.
1039 (C) Enrichment of gene ontology annotation for biological processes among genes that
1040 undergo significant changes in translation (light red – activated translation, dark red –
1041 suppressed translation) in *TSC2*-Null vs WT NPCs. The ten most significant processes are
1042 shown.
1043 (D) Scatterplots from anota2seq analysis of *TSC2*-Null vs WT NPCs (top left and bottom right
1044 panels) and *TSC1*-Null vs WT NPCs (top right and bottom left panels). Transcripts identified
1045 as regulated by translation in anota2seq analysis in the *TSC2*-Null vs WT NPC (top left and
1046 right panels) or *TSC1*-Null vs WT NPC (bottom left and right panels) comparisons are
1047 indicated. Also shown are empirical cumulative distribution functions of the log2 fold changes
1048 in translation for the corresponding gene sets. Grey dots and lines correspond to the
1049 background (i.e. not in gene sets). Significant shifts of gene sets, relative to background, were
1050 determined using Wilcoxon rank-sum test and the resulting p-values are shown.
1051 (E) Venn diagram comparing translationally regulated genes identified in anota2seq analysis
1052 following loss of *TSC1* or *TSC2*.
1053 (F) Enrichments of gene ontology annotation for biological processes among genes identified
1054 as showing consistent regulation in both *TSC1*-Null and *TSC2*-Null NPCs relative to their
1055 controls (same color codes as in panel C).
1056
1057 **Figure 4. Suppressed translation of transcripts encoding ASD- and NDD-associated**
1058 **proteins in *TSC2*-Null NPCs associates with distinct 5'UTR features.**
1059 (A) GSEA analysis of ASD- and NDD-associated genes using anota2seq analysis of
1060 translation (fold-changes) contrasting *TSC2*-Null (-/-) vs WT NPCs. Rankings for ASD- and
1061 NDD-associated genes (ASD72 and NDD373, respectively) were shifted towards the right
1062 denoting suppressed translation. Normalized enrichment scores (NES) and adjusted p-values
1063 are shown.

1064 (B) Scatterplots from anota2seq analysis for *TSC2*-Null vs WT NPCs. High confidence ASD-
1065 and NDD-associated genes (ASD72 and NDD373, respectively) (top left panel) as well as
1066 eIF4E- (middle left panel) or mTOR-sensitive (bottom left panel) transcripts are indicated.
1067 Shown to the right of each panel are corresponding empirical distribution functions together
1068 with associated statistics (as in Figure 3D).
1069 (C-D) Boxplots of 5'UTR lengths (C) and GC-contents (D) (according to the RefSeq database,
1070 version 109.20201120) for ASD- and NDD-associated genes as well as mRNAs translationally
1071 regulated in *TSC2*-Null vs WT NPCs (after excluding ASD- and NDD-associated genes;
1072 background corresponds to mRNAs absent in all subsets). The mean length or GC-contents
1073 for each set are indicated together with p-values from Wilcoxon rank-sum tests.
1074 (E) The proportion of mRNAs harboring upstream open reading frames (uORFs) in their
1075 5'UTRs among subsets of transcripts from C-D. The lower part of the bar graphs corresponds
1076 to uORFs with a strong Kozak context. Differences in proportions of uORFs were assessed
1077 using Fisher's exact tests for the indicated comparisons.
1078
1079 **Figure 5. mTORC1 or MNK1/2 inhibition reverses the TSC2-associated translatome.**
1080 (A and B) Scatterplots from anota2seq analysis of *TSC2*-Null (-/-) NPCs treated with RMC-
1081 6272 vs DMSO (A, top left panel) or eFT-508 vs DMSO (B, top left panel). Sets of transcripts
1082 whose translation was activated or suppressed under each treatment were then assess across
1083 treatments (A and B, bottom panels). Also shown are empirical cumulative distribution
1084 functions (A and B, right panels) of the log2 fold changes in translation for the corresponding
1085 gene sets. Grey dots and lines correspond to the background (i.e. absent in gene sets).
1086 Significant shifts of gene sets, relative to background, were determined using the Wilcoxon
1087 rank-sum test and the resulting p-values are shown.
1088 (C) Assessment of how transcripts whose translation was altered in *TSC2*-Null vs WT NPCs
1089 (top panel, from Figure 3A) are modulated upon treatment with RMC-6272 (bottom left panel)
1090 or eFT-508 (bottom right panel).

1091 (D) Enrichments of gene ontology annotation for biological processes among genes identified
1092 with reversed translation, relative to baseline (*TSC2*-Null vs WT NPCs) that overlap between
1093 RMC-6272 and eFT-508 treatment (same color codes as in Figure 3C).
1094
1095 **Figure 6. mTORC1 or MNK1/2 inhibition reverses translation of transcripts encoding**
1096 **ASD- and NDD-associated proteins in *TSC2*-Null NPCs.**
1097 (A) Scatterplots, showing high confidence ASD- and NDD-associated genes (ASD72 and
1098 NDD373), from anota2seq analysis comparing *TSC2*-Null (-/-) vs WT NPCs (top panel) as well
1099 as RMC-6272 (bottom left) or eFT-508 (bottom right) treated relative to DMSO treated *TSC2*-
1100 Null NPCs are shown. The shape and position of ellipses correspond to the mean and
1101 standard deviation, respectively, for all genes within each gene set.
1102 (B) A Venn diagram of ASD associated genes (ASD72) whose translation was suppressed in
1103 *TSC2*-Null NPC relative to *TSC2*-WT NPCs and reversed by treatment with RMC-6272 or
1104 eFT-508.
1105 (C) Plots denote RT-qPCR analysis from the polysome-associated RNA pool (3 biological
1106 replicates) for 5 ASD- or NDD-associated genes (left) as well as 5 eIF4E-sensitive genes
1107 (right) from the indicated cells and treatments. FC, fold change. Data were normalized to total
1108 mRNA obtained in parallel as well as β-actin *(ACTB)* mRNA expression. P-values from
1109 student's t-test test (*$p<0.05$, **$p<0.01$, ***$p<0.001$) for the indicated comparisons are shown.

Drug Tx[a]	Direction of regulation	Gene set name	# Genes	pV	Gene ID
DMSO	Down (baseline)	ASD72	31	1.72E-07	*MED13, NIPBL, ASH1L, KMT2A, CHD2, EHMT1, KMT5B, CHD8, WAC, RFX3, TLK2, SMARCC2, POGZ, KMT2C, ADNP, KCNB1, MEIS2, ASXL3, DYRK1A, SPAST, SETD5, VEZF1, AUTS2, NRXN1, TCF7L2, TAOK1, NF1, ZBTB20, MED23, KDM5B, DNMT3A*
RMC	Up	ASD72	28	1.78E-11	*MED13, NIPBL, ASH1L, KMT2A, CHD2, EHMT1, KMT5B, CHD8, WAC, RFX3, TLK2, POGZ, KMT2C, ADNP, MEIS2, ASXL3, DYRK1A, SPAST, SETD5, VEZF1, AUTS2, NRXN1, TCF7L2, TAOK1, NF1, MED23, KDM5B, DNMT3A*
eFT-508	Up	ASD72	18	8.63E-06	*MED13, NIPBL, ASH1L, KMT2A, CHD2, KMT5B, WAC, RFX3, KMT2C, MEIS2, ASXL3, SPAST, VEZF1, AUTS2, NRXN1, TCF7L2, TAOK1, NF1*
n/a	Down (baseline)	NDD373	138	2.59E-19	*MED13, NIPBL, SMC3, CNOT1, KMT2E, UBTF, KDM3B, TRRAP, USP7, ASH1L, KMT2A, CREBBP, KAT6A, SIN3A, CHD2, ARID1A, SPEN, EHMT1, TLE3, UBR5, CHD7, KMT5B, HIVEP2, CHD8, WAC, ZNF462, NSD1, ARID2, GATAD2B, FBXO11, TAB2, HDAC2, KMT2D, ZNF148, RFX3, TBL1XR1, ZEB2, SETBP1, PHIP, TLK2, RAI1, KIF5C, SMARCC2, SON, STAG1, POGZ, ZMYND11, KIF11, KMT2C, ADNP, KCNB1, COL4A1, KAT6B, SCN8A, ZMYND8, RFX7, PHF12, ZFHX3, SHOC2, TRIO, SOS1, ZNF292, ZFHX4, GNB1, SETD1B, TANC2, KIF2A, ARIH1, SOX9, ACVR2A, TNRC6B, SET, MEIS2, CTNND1, SMARCE1, GLI3, YY1, ASXL3, PDE4D, SETD2, SYNCRIP, BRAF, MAP3K7, DYRK1A, WDR48, TCF4, SRP54, SMAD4, SPAST, SETD5, HNRNPD, PIK3R1, SNAP25, FBXW7, VEZF1, SRSF1, KLF7, TOP2B, ZMIZ1, AUTS2, NRXN1, TRIM8, PPP2CA, CHAMP1, TCF7L2, TAOK1, ATF2, ZBTB10, NF1, SATB1, CSNK2A1, BICD2, CAPRIN1, ZBTB20, CDK13, ZMYM2, GABRB3, CBX5, TCF12, MAP2K1, MYCN, CDK8, SOX11, SYT1, TRPM3, RAC1, MSL2, ABCC9, MED23, DNM1L, KLHL20, TNPO3, KDM5B, KBTBD7, PPM1D, KRAS, DNMT3A, MIB1*
RMC	Up	NDD373	96	4.37E-18	*MED13, NIPBL, SMC3, CNOT1, KMT2E, UBTF, TRRAP, USP7, ASH1L, KMT2A, CREBBP, KAT6A, SIN3A, CHD2, EHMT1, TLE3, UBR5, CHD7, KMT5B, HIVEP2, CHD8, WAC, ZNF462, NSD1, ARID2, FBXO11, TAB2, KMT2D, ZNF148, RFX3, ZEB2, SETBP1, TLK2, RAI1, KIF5C, SON, STAG1, POGZ, ZMYND11, KIF11, KMT2C, ADNP, COL4A1, KAT6B, SCN8A, ZMYND8, PHF12, ZFHX3, SHOC2, TRIO, SOS1, ZNF292, SETD1B, TANC2, ARIH1, SOX9, ACVR2A, TNRC6B, MEIS2, CTNND1, YY1, ASXL3, PDE4D, SETD2, MAP3K7, DYRK1A, WDR48, SRP54, SPAST, SETD5, PIK3R1, SNAP25, VEZF1, KLF7, ZMIZ1, AUTS2, NRXN1, PPP2CA, CHAMP1, TCF7L2, TAOK1, ZBTB10, NF1, SATB1, CDK13, MAP2K1, MYCN, SYT1, TRPM3, MSL2, ABCC9, MED23, KLHL20, KDM5B, PPM1D, DNMT3A*
eFT-508	Up	NDD373	69	1.48E-10	*MED13, NIPBL, SMC3, KMT2E, ASH1L, KMT2A, KAT6A, SIN3A, CHD2, SPEN, UBR5, KMT5B, HIVEP2, WAC, ZNF462, ARID2, FBXO11, TAB2, KMT2D, ZNF148, RFX3, ZEB2, KIF5C, STAG1, ZMYND11, KIF11, KMT2C, KAT6B, SCN8A, RFX7, ZFHX3, SHOC2, TRIO, SOS1, ZNF292, TANC2, KIF2A, ARIH1, ACVR2A, MEIS2, ASXL3, PDE4D, SETD2, BRAF, MAP3K7, WDR48, SRP54, SPAST, PIK3R1, SNAP25, VEZF1, ZMIZ1, AUTS2, NRXN1, CHAMP1, TCF7L2, TAOK1, ATF2, ZBTB10, NF1, SATB1, CDK13, GABRB3, SYT1, ABCC9, DNM1L, KLHL20, TNPO3, MIB1*
n/a	Down (baseline)	EPI	22	5.82E-03	*KMT2E, DHX57, TTF1, KDM5B, TTI1, PCDH19, NCOA1, CDKAL1, KANSL1L, DYRK1A, CHD9, ORC2, FAM184A, TUT7, BIRC6, ALKBH8, SETD1B, ANK1, SLC6A16, BPTF, ZSCAN26, PMFBP1*
RMC	Up	EPI	19	6.97E-05	*KMT2E, DHX57, KDM5B, TTI1, PCDH19, NCOA1, KANSL1L, DYRK1A, CHD9, ORC2, FAM184A, TUT7, BIRC6, ALKBH8, SETD1B, SLC6A16, BPTF, ZSCAN26, PMFBP1*
eFT-508	Up	EPI	11	3.32E-02	*KMT2E, PCDH19, NCOA1, CHD9, FAM184A, TUT7, BIRC6, ALKBH8, SLC6A16, BPTF, PMFBP1*

Table 1. Gene set enrichment analysis of translationally downregulated genes in *TSC2*-Null NPCs related to ASD, NDD and epilepsy. [a]Drug Tx, treatment: DMSO, 10 nM RMC-6272 or 50 nM eFT-508; n/a, not applicable; pV, p-value; ASD72, 72 gene variants (false discovery rate (FDR)<0.001) identified in patients with autism spectrum disorder; NDD373, 373 gene variants (FDR<0.001) identified in patients with neurodevelopmental disorders [38]; EPI83, 83 gene variants identified in full epilepsy cohort [42].

Figure 1

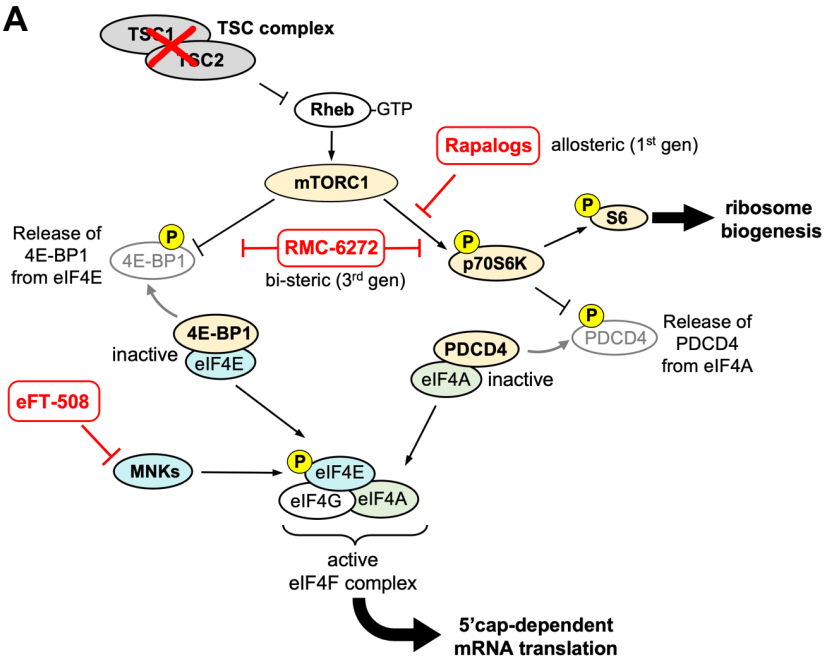
A
TSC1
TSC2
TSC complex
Rheb
-GTP
Rapalogs
allosteric (1st gen)
mTORC1
P
S6
ribosome biogenesis
Release of 4E-BP1 from eIF4E
P
4E-BP1
RMC-6272
bi-steric (3rd gen)
P
p70S6K
P
PDCD4
Release of PDCD4 from eIF4A
4E-BP1
inactive
eIF4E
PDCD4
eIF4A
inactive
eFT-508
MNKs
P
eIF4E
eIF4G
eIF4A
active eIF4F complex
5'cap-dependent mRNA translation

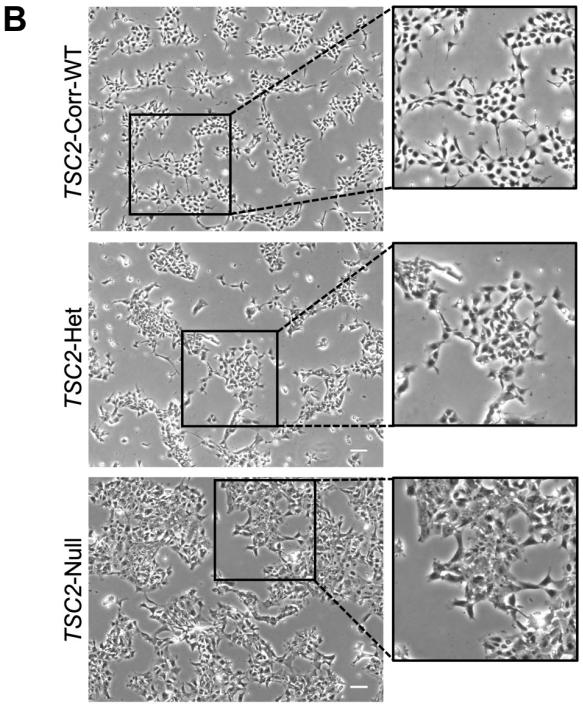
B
TSC2-Corr-WT
TSC2-Het
TSC2-Null

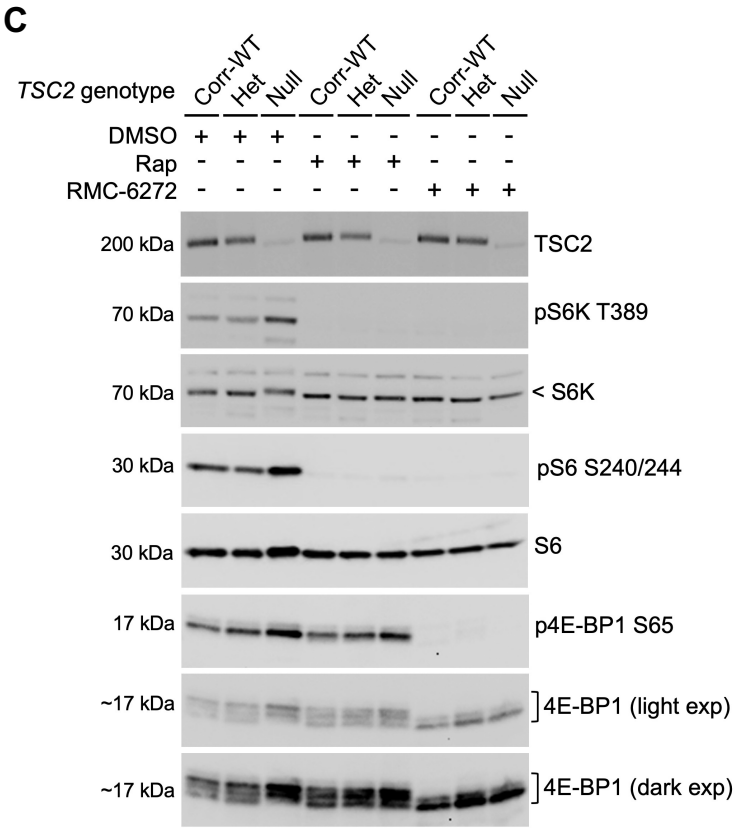
C
TSC2 genotype
Corr-WT
Het
Null
Corr-WT
Het
Null
Corr-WT
Het
Null
DMSO + + + - - - - - -
Rap - - - + + + - - -
RMC-6272 - - - - - - + + +
200 kDa
TSC2
70 kDa
pS6K T389
70 kDa
< S6K
30 kDa
pS6 S240/244
30 kDa
S6
17 kDa
p4E-BP1 S65
~17 kDa
4E-BP1 (light exp)
~17 kDa
4E-BP1 (dark exp)

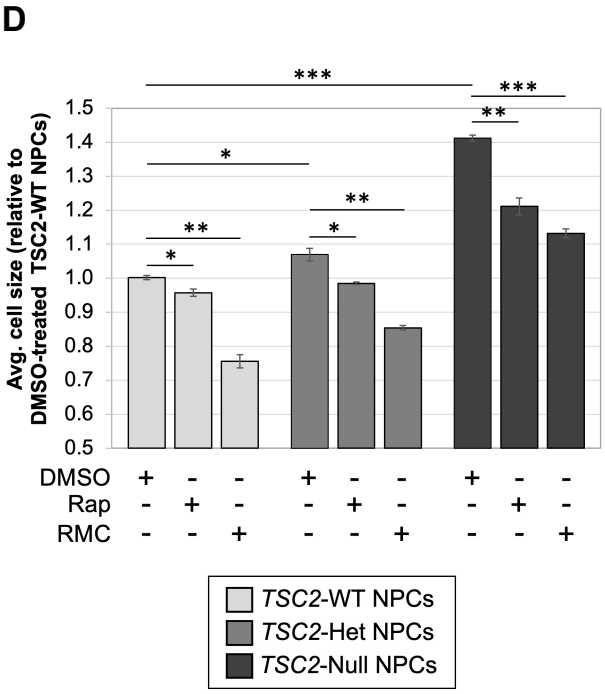
D
Avg. cell size (relative to DMSO-treated TSC2-WT NPCs)
1.5
1.4
1.3
1.2
1.1
1.0
0.9
0.8
0.7
0.6
0.5
***
***
**
*
**
*
**
*
*
DMSO + - - + - - + - -
Rap - + - - + - - + -
RMC - - + - - + - - +
TSC2-WT NPCs
TSC2-Het NPCs
TSC2-Null NPCs

Figure 2

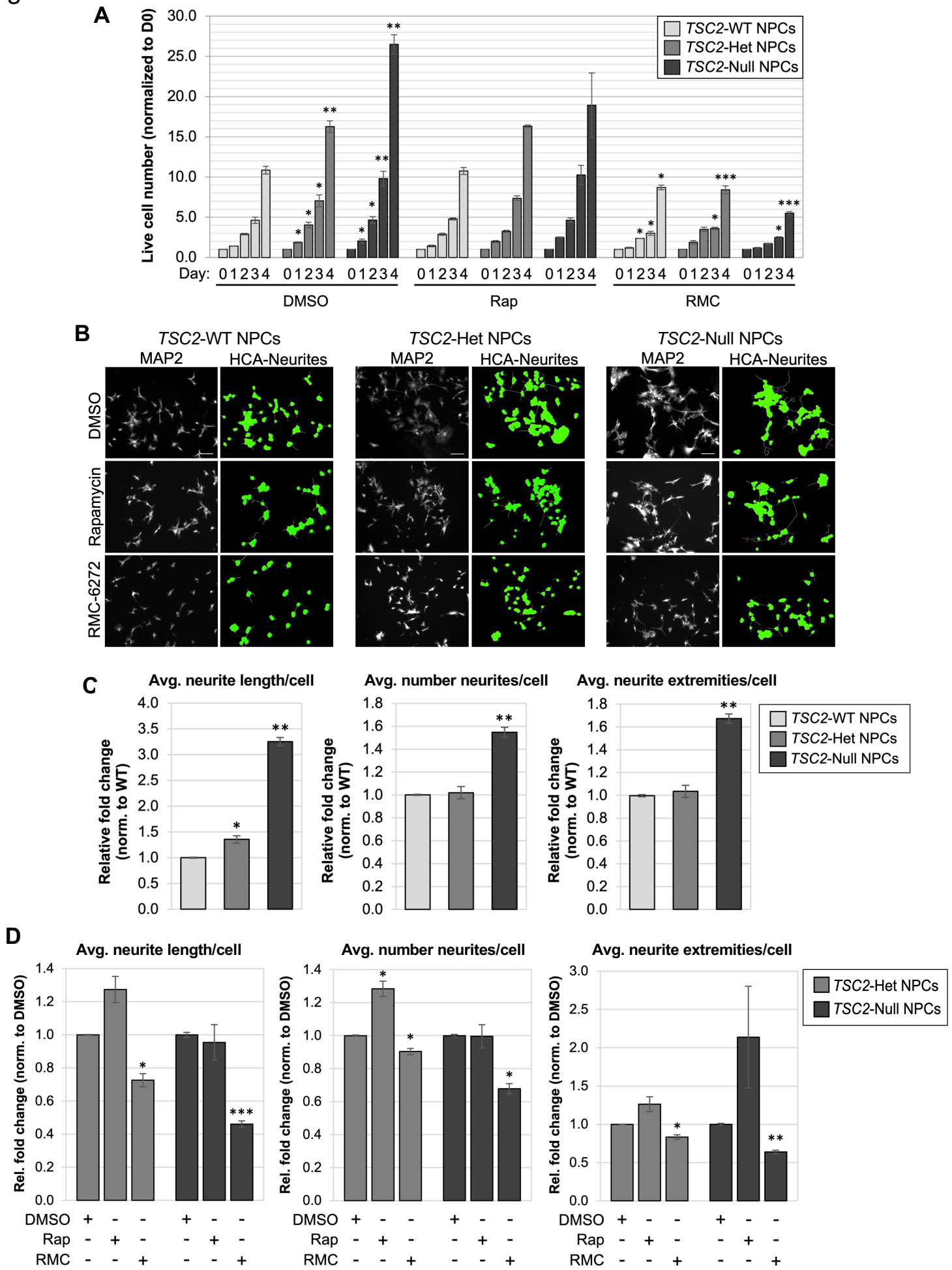
A
Live cell number (normalized to D0)
30.0
25.0
20.0
15.0
10.0
5.0
0.0
TSC2-WT NPCs
TSC2-Het NPCs
TSC2-Null NPCs
Day: 0 1 2 3 4 0 1 2 3 4 0 1 2 3 4 0 1 2 3 4 0 1 2 3 4 0 1 2 3 4 0 1 2 3 4 0 1 2 3 4
DMSO
Rap
RMC
B
TSC2-WT NPCs
TSC2-Het NPCs
TSC2-Null NPCs
MAP2
HCA-Neurites
DMSO
Rapamycin
RMC-6272
C
Avg. neurite length/cell
Avg. number neurites/cell
Avg. neurite extremities/cell
Relative fold change (norm. to WT)
TSC2-WT NPCs
TSC2-Het NPCs
TSC2-Null NPCs
D
Avg. neurite length/cell
Avg. number neurites/cell
Avg. neurite extremities/cell
Rel. fold change (norm. to DMSO)
TSC2-Het NPCs
TSC2-Null NPCs
DMSO
Rap
RMC

Figure 3

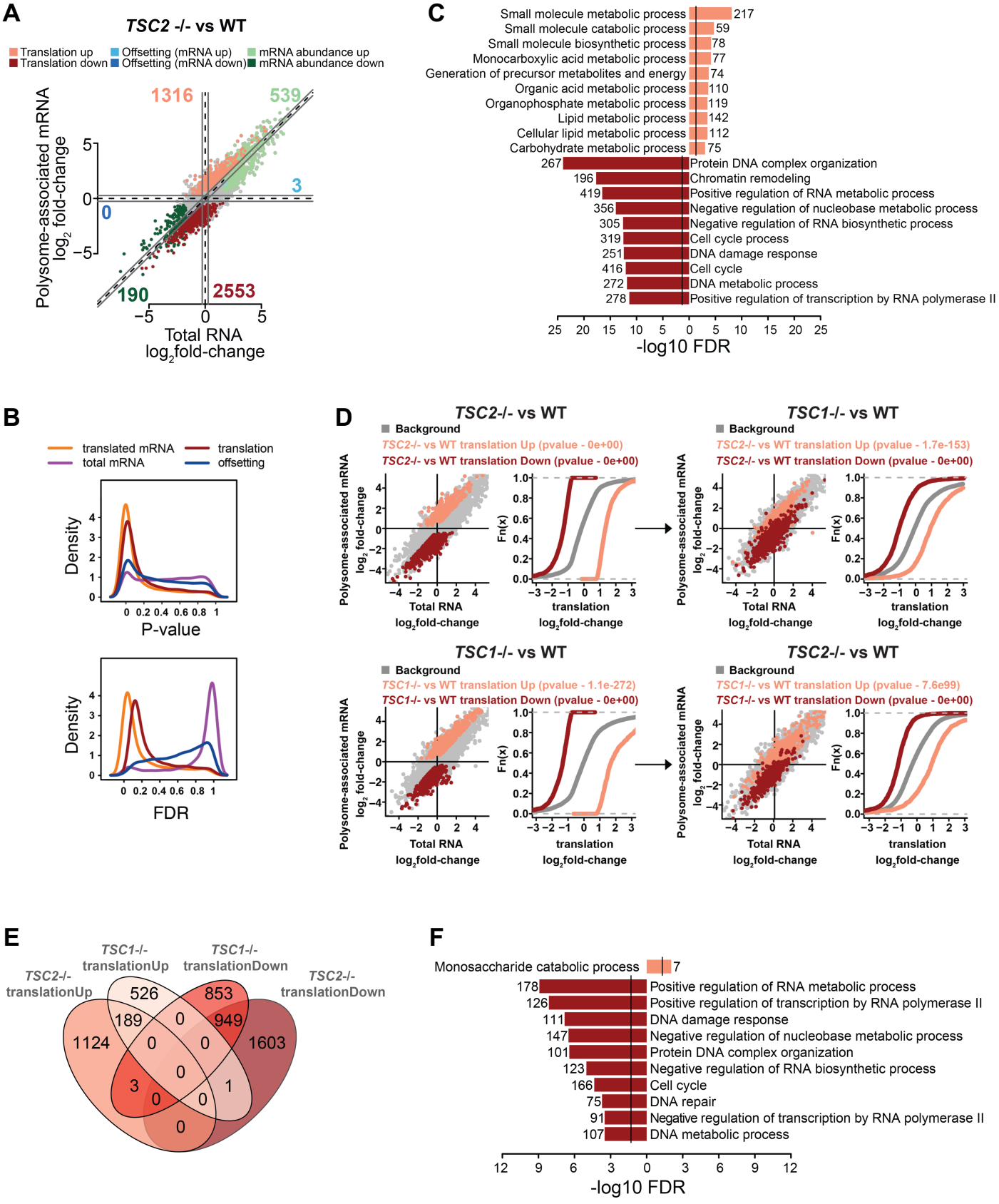
A
TSC2 -/- vs WT
Translation up
Translation down
Offsetting (mRNA up)
Offsetting (mRNA down)
mRNA abundance up
mRNA abundance down
1316
539
3
0
190
2553
Polysome-associated mRNA log2 fold-change
Total RNA log2fold-change
C
Small molecule metabolic process 217
Small molecule catabolic process 59
Small molecule biosynthetic process 78
Monocarboxylic acid metabolic process 77
Generation of precursor metabolites and energy 74
Organic acid metabolic process 110
Organophosphate metabolic process 119
Lipid metabolic process 142
Cellular lipid metabolic process 112
Carbohydrate metabolic process 75
267 Protein DNA complex organization
196 Chromatin remodeling
419 Positive regulation of RNA metabolic process
356 Negative regulation of nucleobase metabolic process
305 Negative regulation of RNA biosynthetic process
319 Cell cycle process
251 DNA damage response
416 Cell cycle
272 DNA metabolic process
278 Positive regulation of transcription by RNA polymerase II
-log10 FDR
B
translated mRNA
total mRNA
translation
offsetting
Density
P-value
FDR
D
TSC2-/- vs WT
Background
TSC2-/- vs WT translation Up (pvalue - 0e+00)
TSC2-/- vs WT translation Down (pvalue - 0e+00)
TSC1-/- vs WT
Background
TSC2-/- vs WT translation Up (pvalue - 1.7e-153)
TSC2-/- vs WT translation Down (pvalue - 0e+00)
TSC1-/- vs WT
Background
TSC1-/- vs WT translation Up (pvalue - 1.1e-272)
TSC1-/- vs WT translation Down (pvalue - 0e+00)
TSC2-/- vs WT
Background
TSC1-/- vs WT translation Up (pvalue - 7.6e99)
TSC1-/- vs WT translation Down (pvalue - 0e+00)
Polysome-associated mRNA log2 fold-change
Total RNA log2fold-change
Fn(x)
translation log2fold-change
E
TSC2-/- translationUp
TSC1-/- translationUp
TSC1-/- translationDown
TSC2-/- translationDown
526
853
189
949
1124
1603
F
Monosaccharide catabolic process 7
178 Positive regulation of RNA metabolic process
126 Positive regulation of transcription by RNA polymerase II
111 DNA damage response
147 Negative regulation of nucleobase metabolic process
101 Protein DNA complex organization
123 Negative regulation of RNA biosynthetic process
166 Cell cycle
75 DNA repair
91 Negative regulation of transcription by RNA polymerase II
107 DNA metabolic process
-log10 FDR

Figure 4

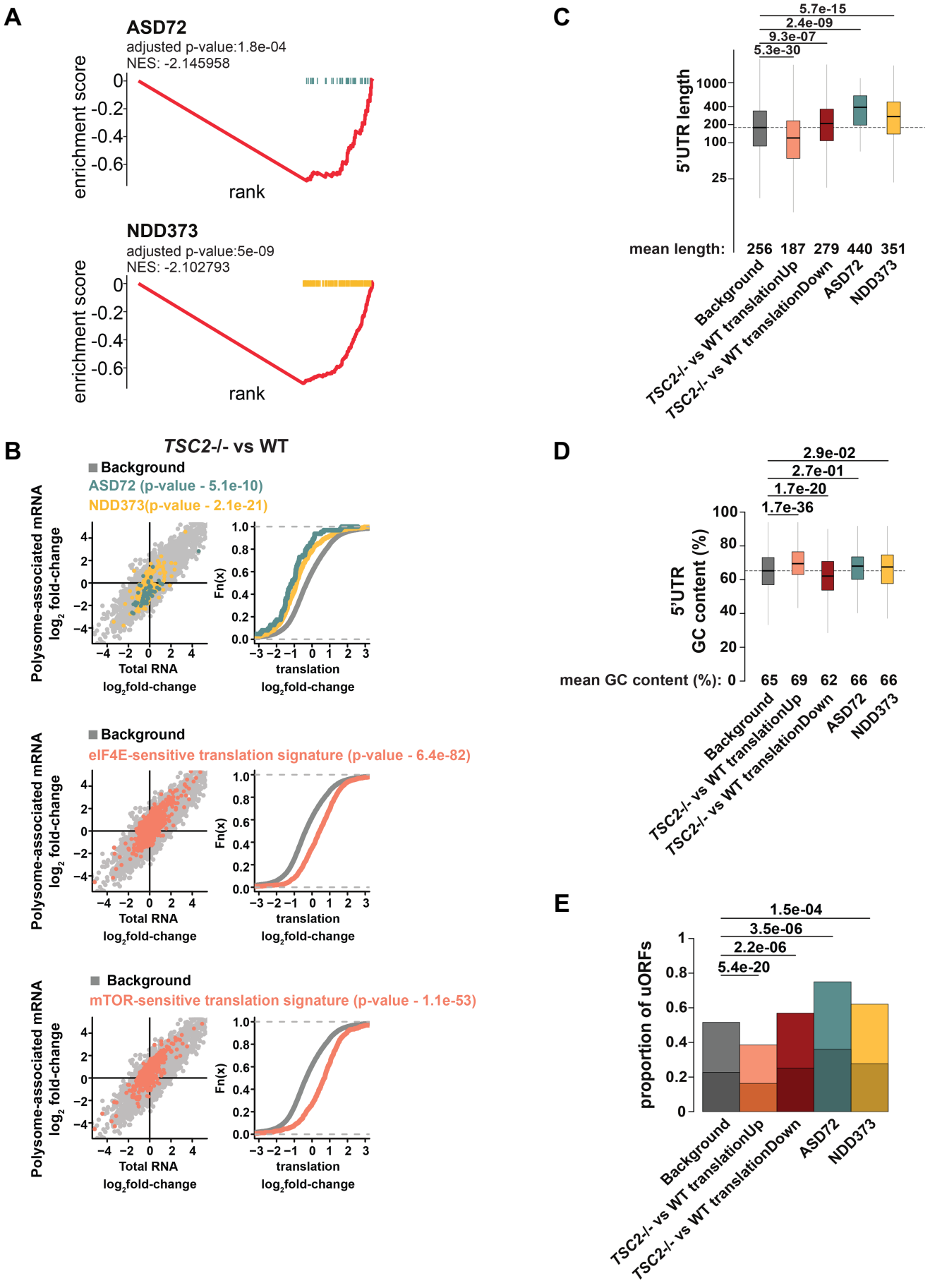
A
ASD72
adjusted p-value:1.8e-04
NES: -2.145958
enrichment score
rank
NDD373
adjusted p-value:5e-09
NES: -2.102793
enrichment score
rank
B
TSC2-/- vs WT
Background
ASD72 (p-value - 5.1e-10)
NDD373(p-value - 2.1e-21)
Polysome-associated mRNA log2 fold-change
Total RNA log2fold-change
Fn(x)
translation log2fold-change
Background
eIF4E-sensitive translation signature (p-value - 6.4e-82)
Background
mTOR-sensitive translation signature (p-value - 1.1e-53)
C
5.7e-15
2.4e-09
9.3e-07
5.3e-30
5'UTR length
mean length: 256 187 279 440 351
Background
TSC2-/- vs WT translationUp
TSC2-/- vs WT translationDown
ASD72
NDD373
D
2.9e-02
2.7e-01
1.7e-20
1.7e-36
5'UTR GC content (%)
mean GC content (%): 65 69 62 66 66
Background
TSC2-/- vs WT translationUp
TSC2-/- vs WT translationDown
ASD72
NDD373
E
1.5e-04
3.5e-06
2.2e-06
5.4e-20
proportion of uORFs
Background
TSC2-/- vs WT translationUp
TSC2-/- vs WT translationDown
ASD72
NDD373

Figure 5

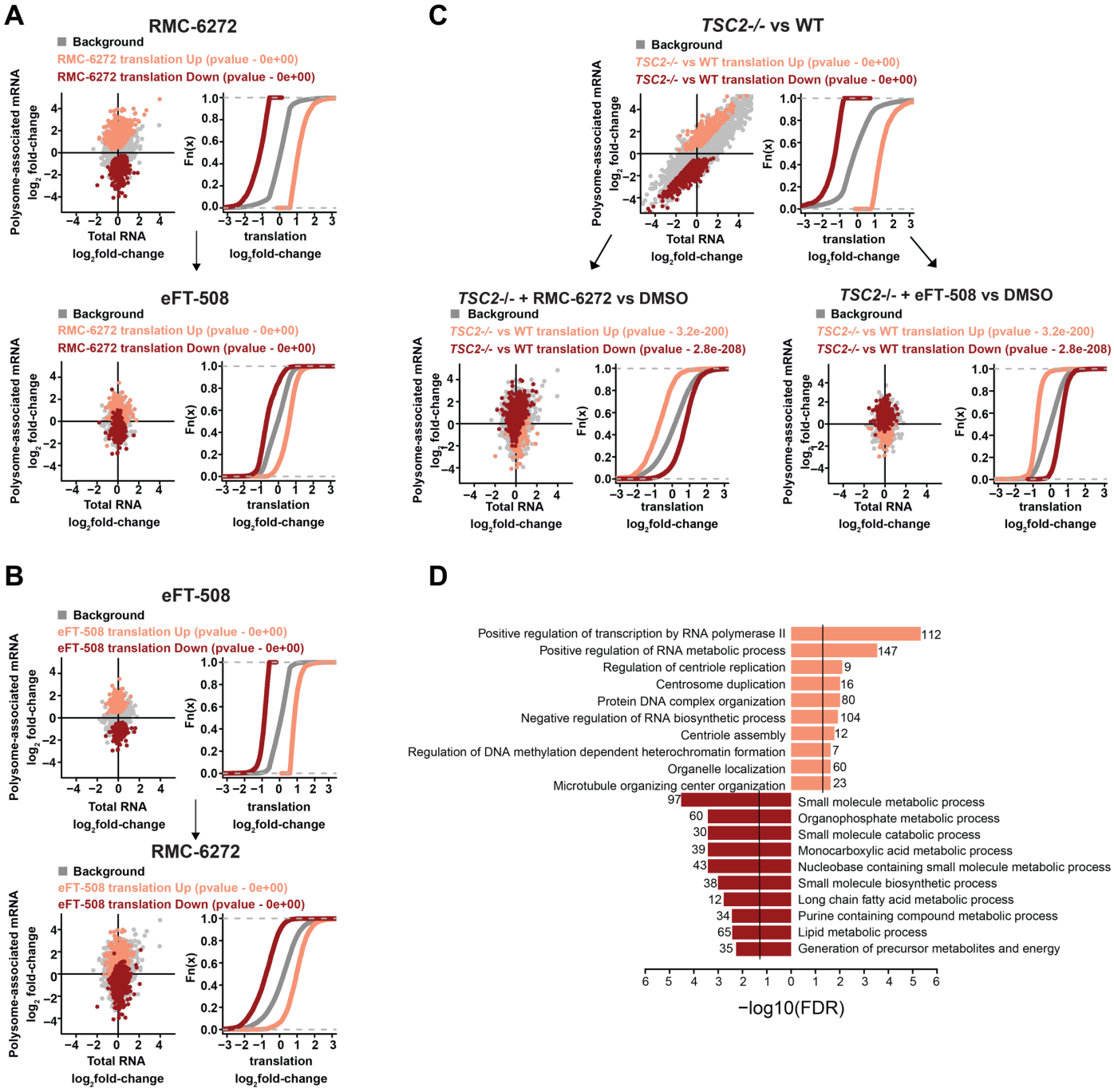
A
RMC-6272
Background
RMC-6272 translation Up (pvalue - 0e+00)
RMC-6272 translation Down (pvalue - 0e+00)
Polysome-associated mRNA log2 fold-change
Total RNA log2fold-change
Fn(x)
translation log2fold-change
eFT-508
Background
RMC-6272 translation Up (pvalue - 0e+00)
RMC-6272 translation Down (pvalue - 0e+00)
B
eFT-508
Background
eFT-508 translation Up (pvalue - 0e+00)
eFT-508 translation Down (pvalue - 0e+00)
RMC-6272
Background
eFT-508 translation Up (pvalue - 0e+00)
eFT-508 translation Down (pvalue - 0e+00)
C
TSC2-/- vs WT
Background
TSC2-/- vs WT translation Up (pvalue - 0e+00)
TSC2-/- vs WT translation Down (pvalue - 0e+00)
TSC2-/- + RMC-6272 vs DMSO
Background
TSC2-/- vs WT translation Up (pvalue - 3.2e-200)
TSC2-/- vs WT translation Down (pvalue - 2.8e-208)
TSC2-/- + eFT-508 vs DMSO
Background
TSC2-/- vs WT translation Up (pvalue - 3.2e-200)
TSC2-/- vs WT translation Down (pvalue - 2.8e-208)
D
Positive regulation of transcription by RNA polymerase II 112
Positive regulation of RNA metabolic process 147
Regulation of centriole replication 9
Centrosome duplication 16
Protein DNA complex organization 80
Negative regulation of RNA biosynthetic process 104
Centriole assembly 12
Regulation of DNA methylation dependent heterochromatin formation 7
Organelle localization 60
Microtubule organizing center organization 23
97 Small molecule metabolic process
60 Organophosphate metabolic process
30 Small molecule catabolic process
39 Monocarboxylic acid metabolic process
43 Nucleobase containing small molecule metabolic process
38 Small molecule biosynthetic process
12 Long chain fatty acid metabolic process
34 Purine containing compound metabolic process
65 Lipid metabolic process
35 Generation of precursor metabolites and energy
−log10(FDR)

Figure 6

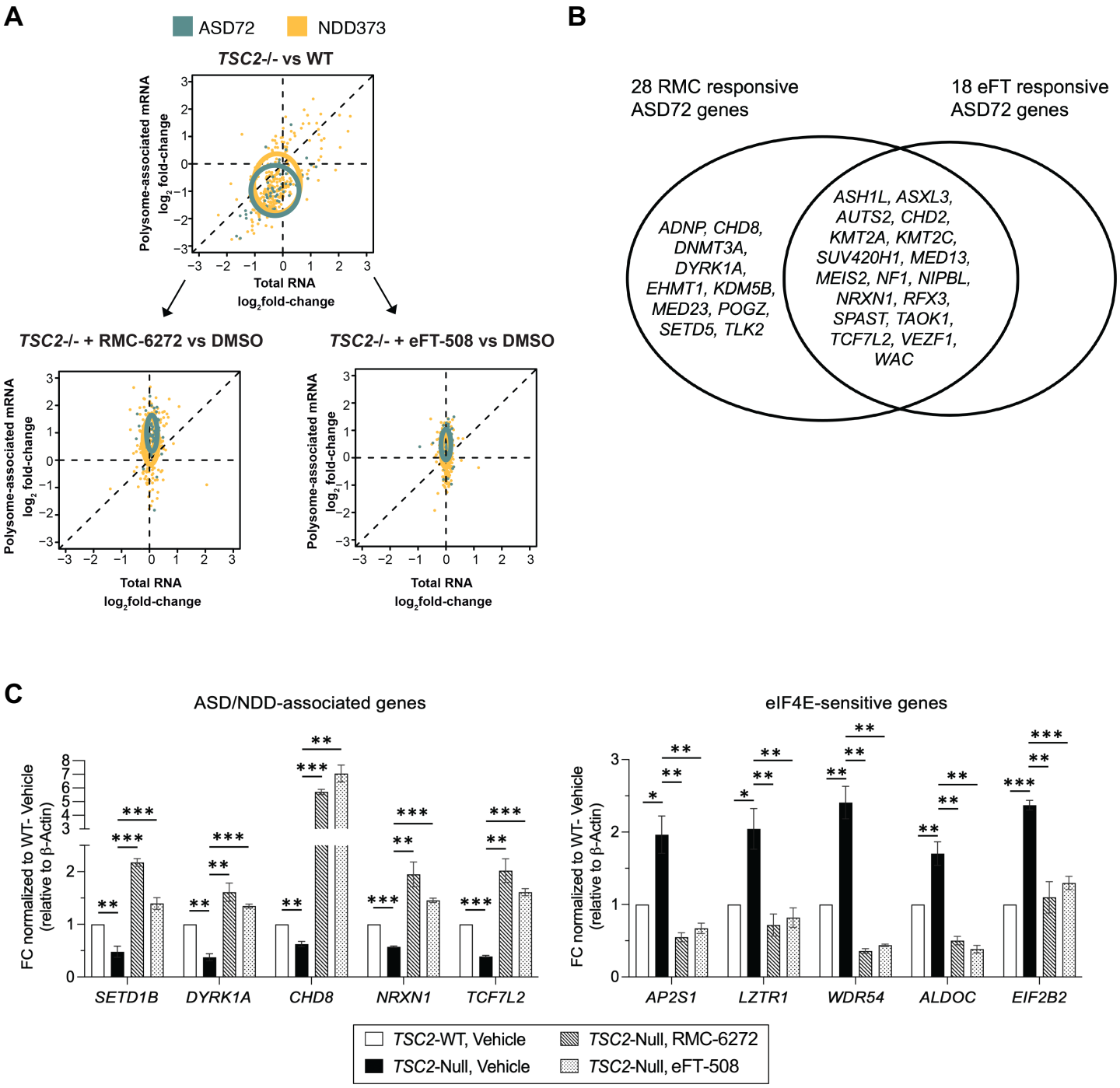
A
ASD72
NDD373
TSC2-/- vs WT
Polysome-associated mRNA log2 fold-change
Total RNA log2fold-change
TSC2-/- + RMC-6272 vs DMSO
TSC2-/- + eFT-508 vs DMSO
B
28 RMC responsive ASD72 genes
18 eFT responsive ASD72 genes
ADNP, CHD8, DNMT3A, DYRK1A, EHMT1, KDM5B, MED23, POGZ, SETD5, TLK2
ASH1L, ASXL3, AUTS2, CHD2, KMT2A, KMT2C, SUV420H1, MED13, MEIS2, NF1, NIPBL, NRXN1, RFX3, SPAST, TAOK1, TCF7L2, VEZF1, WAC
C
ASD/NDD-associated genes
eIF4E-sensitive genes
FC normalized to WT- Vehicle (relative to β-Actin)
SETD1B
DYRK1A
CHD8
NRXN1
TCF7L2
AP2S1
LZTR1
WDR54
ALDOC
EIF2B2
TSC2-WT, Vehicle
TSC2-Null, Vehicle
TSC2-Null, RMC-6272
TSC2-Null, eFT-508